The Astrophysical Journal, 616:71–85, 2004 November 20

THE REST-FRAME OPTICAL PROPERTIES OF SCUBA GALAXIES

Ian Smail,[1] S. C. Chapman,[2] A. W. Blain,[2] and R. J. Ivison[3,4]

Received 2004 May 28; accepted 2004 July 23

ABSTRACT

We present optical and near-infrared photometry for a sample of 96 dusty, far-infrared–luminous galaxies. We have precise spectroscopic redshifts for all these galaxies, yielding a median redshift of $\langle z \rangle = 2.2$. The majority, 78, are submillimeter-detected galaxies lying at $z = 0.2-3.6$, while the remaining 18 are optically faint μJy radio galaxies at $z = 0.9-3.4$ that are proposed to be similarly luminous, dusty galaxies whose dust emission is too hot to be detected in the submillimeter waveband. We compare the photometric and morphological properties of these distant, ultraluminous galaxies with local samples of dusty, luminous galaxies. We confirm that spectroscopically identified far-infrared–luminous galaxies at $z > 1$ display a wide variety in their optical–near-infrared and near-infrared colors, with only a modest proportion red enough to classify as unusually red. We show that, on average, luminous, high-redshift dusty galaxies are both brighter and redder in rest-frame optical passbands than comparable samples of UV-selected star-forming galaxies at similar redshifts. Archival *Hubble Space Telescope* ACS imaging of 20 of our galaxies demonstrates both morphological indications of mergers and interactions, which may have triggered their luminous far-infrared activity, and structured dust distributions within these galaxies. We derive a near-infrared Hubble diagram for far-infrared–luminous galaxies. This shows that this population is typically fainter than high-luminosity radio galaxies at similar redshifts and exhibits significantly more scatter in their *K*-band magnitudes. The rest-frame optical luminosities of the far-infrared–luminous population are comparable to those of local ultraluminous infrared galaxies, although their far-infrared luminosities are several times higher. The typical extinction-corrected optical luminosity of the high-redshift population, assuming passive evolution, provides a good fit to the bright end of the luminosity function of luminous spheroidal galaxies seen in rich clusters at intermediate redshifts. This adds to the growing body of evidence showing that these high-redshift, far-infrared–luminous sources identify star formation and active galactic nucleus–fueling events in the early life of massive galaxies in the universe.

Subject headings: cosmology: observations — galaxies: evolution — galaxies: formation — infrared: galaxies

On-line material: color figures, machine-readable table

1. INTRODUCTION

Ten billion years ago, at a redshift of $z \sim 2.5$, the universe was a much more active place. This is the era of the peak activity in quasars (Boyle et al. 2000), and recent surveys suggest that it coincides with the peak activity in other galaxy populations. These include surveys for star-forming galaxies selected photometrically either in their rest-frame UV continuum light (Shapley et al. 2001; Steidel et al. 2004) or in their rest-frame optical continuum light (Franx et al. 2003; Daddi et al. 2003, 2004; Cimatti et al. 2004) or through their intense far-infrared/radio emission (Chapman et al. 2003a). Taken together, the results from these surveys provide a well-stocked, rich, and apparently disparate zoo of galaxies and active galactic nuclei (AGNs) at this epoch. This enables us to investigate the relationships between these different populations through direct comparison of their physical properties, such as space densities, masses, clustering strength, stellar ages, and luminosities. In this way we can test whether these different classes represent, for example, a mass sequence or whether they are different stages in the life of a single population, similar to the unification schemes that have been suggested to connect local ultraluminous infrared galaxies (ULIRGs) and QSOs (Sanders et al. 1988).

This paper focuses on determining the photometric properties in the rest-frame optical wavebands of a large sample of far-infrared–luminous galaxies at $z \sim 2.5$ with complete redshift coverage (Chapman et al. 2003a, 2004a, 2004b). These high-redshift, far-infrared–luminous galaxies are selected using two independent selection criteria. The larger subsample is based on a spectroscopic survey for optically faint, radio-selected sources with submillimeter (submm) fluxes above $\sim$5 mJy (Chapman et al. 2003a, 2004a). These are "classical" submm (or SCUBA) galaxies (SMGs), which appear to be a population of highly obscured starbursts and starburst/AGNs at high redshifts (Bertoldi et al. 2000; Smail et al. 2002a; Ivison et al. 2002; Webb et al. 2003; Chapman et al. 2003a, 2004a; Borys et al. 2004; Dannerbauer et al. 2004) and are thought to be intimately linked with the formation of massive galaxies (Frayer et al. 1998, 1999, 2004a; Gear et al. 2000; Lutz et al. 2001; Genzel et al. 2003; Blain et al. 2004b; Greve et al. 2004b). The second, smaller subsample comprises similarly optically faint μJy radio sources (OFRGs) with spectroscopic redshifts that place them at redshifts comparable to those of the SMGs, but with limits on their submm flux that preclude them being luminous submm sources (Chapman et al. 2004b). Although they are undetected in the submm waveband, these galaxies are still proposed to be luminous far-infrared sources but with higher characteristic dust temperatures than those exhibited by the

[1] Institute for Computational Cosmology, University of Durham, South Road, Durham DH1 3LE, UK.
[2] California Institute of Technology, Pasadena, CA 91125.
[3] Astronomy Technology Centre, Royal Observatory, Blackford Hill, Edinburgh EH9 3HJ, UK.
[4] Institute for Astronomy, University of Edinburgh, Royal Observatory, Blackford Hill, Edinburgh EH9 3HJ, UK.

submm-detected population (Blain et al. 2004a; Chapman et al. 2004b). This proposal will be tested through measurement of the mid-infrared properties of these galaxies with the *Spitzer Space Telescope* (*Spitzer*) in the near future. Even if this claim proves to be erroneous, their inclusion in our analysis does not qualitatively change any of the conclusions in this paper.

The selection function for this far-infrared–luminous sample is very broad, so to relate their properties to those of the populations of $z \sim 2.5$ galaxies and AGNs selected via different techniques, we must have redshift information. With this we can isolate those galaxies in the relevant redshift range and simply compare their observed properties with other populations at these redshifts, including BX/BM galaxies (Steidel et al. 2004), very red near-infrared galaxies at $z \sim 2$ (Franx et al. 2003), or QSOs (Boyle et al. 2000). We are particularly interested in testing the relationship between these populations by comparing their stellar masses, as well as testing the possible connection between SMGs/OFRGs and the formation phase of the luminous, evolved elliptical galaxies that populate high-density regions out to at least $z \sim 1$. For galaxy populations at $z \sim 2$ these tests can be done using characteristics derived from the rest-frame optical properties of the galaxies, which are accessible in the near-infrared wavebands from the ground. Further progress will come from space-based, mid-infrared observations with *Spitzer*. These have the ability to probe the rest-frame near-infrared emission from these galaxies, providing an even more reliable measure of the luminosities of their stellar populations.

In this paper we collect optical and near-infrared photometry for a sample of 96 submm- or radio-selected, far-infrared–luminous galaxies with precise spectroscopic redshifts. We use these data to discuss the rest-frame optical continuum properties of these galaxies and compare them with similar observations of both low- and high-redshift galaxy populations. We use our near-infrared photometry to estimate the likely optical luminosities and model their colors to derive a typical age and dust extinction for the population as a whole. We then examine the evolution of these galaxies to determine the properties of possible descendants at lower redshifts.

The paper is structured as follows: § 2 details our observations and their reduction, while § 3 analyses these and gives the results derived from these data. Section 4 discusses these results and summarizes our main conclusions. We assume throughout a cosmology with $h_{100} = 0.71$, $\Omega_0 = 0.27$, and $\Omega_\Lambda = 0.73$.

2. OBSERVATIONS AND REDUCTION

Our analysis uses new near-infrared imaging in conjunction with archival observations and published optical and near-infrared photometry to produce a catalog of optical/near-infrared colors for spectroscopically identified submm- and radio-selected sources from the surveys of Chapman et al. (2003a, 2004a, 2004b). These surveys cover seven fields: the Canada-France Redshift Survey (CFRS) 03, Lockman Hole, Hubble Deep Field–North (HDF-N), SA 13, CFRS 14, ELAIS-N2, and SA 22, and we discuss the data available for each field below. We supplement these with *IJK* photometry of the five well-studied submm galaxies with redshifts in the SCUBA cluster lens survey (Smail et al. 2002a), as given by Frayer et al. (2004a).

2.1. *Ground-based Optical and Near-Infrared Imaging*

I- and *K*-band photometry (in 4″ diameter apertures) is available for the sources in the ELAIS-N2 and the Lockman Hole fields from Ivison et al. (2002), and we adopt the same large photometric aperture for this work. The choice of aperture size is driven by our desire to obtain representative colors for the entirety of these extended (median optical size of 2.″3; see § 3) and sometimes morphologically complex galaxies (Chapman et al. 2003b). There are two penalties for this choice: first, the apparent point-source sensitivity in the aperture is brighter than it would otherwise be, and second, in about 15% of cases our photometry might suffer from contamination by probably unrelated bright galaxies. Where contamination *may* have occurred we flag these objects in our catalog. However, we have retained these objects in our analysis, as we have confirmed that their presence does not affect any of our qualitative conclusions.

For several of the submm sources in the CFRS 03 and CFRS 14 fields *I*/*K*-band photometry was published in Webb et al. (2003) and Clements et al. (2004) (but using 3″ diameter apertures). We have remeasured the photometry for these sources (and our new radio sources and submm IDs in these fields) in 4″ diameter apertures. In addition, for the remaining fields without published photometry (HDF, SA 13, and SA 22) we have measured the 4″ diameter photometry off new and available archival imaging. We now discuss this imaging on a field-by-field basis.

For all of our spectroscopic sample in the ELAIS-N2 and the Lockman Hole fields we rely on the *I*- and *K*-band imaging published by Ivison et al. (2002). For the CFRS 03 field we have retrieved and rereduced the *K*-band imaging used by Webb et al. (2003) from the CFHT archive. New *J*/*K*-band observations of the Lockman Hole and CFRS 03 fields were obtained with the wide-field WIRC2 near-infrared imager (Eikenberry et al. 2004) on the Palomar Hale 5 m telescope on the nights of 2004 January 6–8. The seeing was 0.″9–2.″0, and the exposure times were 3.3 ks for the *K* band and 6.6 ks in the *J* band, in nonphotometric conditions. Nevertheless, the wide field of view of WIRC2 (8.′5 × 8.′5) makes it relatively simple to derive zero points for these exposures from Two Micron All Sky Survey (2MASS) stars in these regions. We estimate the precision of the zero points to be $\lesssim 0.04$ mag on the basis of the scatter between stars and the typical depth of these observations to be $J \sim 22.3$ and $K \sim 20.8$ (3 σ).

New *J*/*K*-band imaging of the CFRS 14 and SA 13 fields was also taken with the WIRC2 imager on the nights of 2004 January 8–9. The total exposure times are 11.4 ks in *J* and 3.3 ks in the *K* band for CFRS 14 and 14.0 ks in *J* and 10.5 ks in the *K* band for SA 13. The conditions were nonphotometric, but again the data can be reliably calibrated from 2MASS stars serendipitously lying within the large WIRC2 field to a precision of $\lesssim 0.04$ mag. The 3 σ limiting magnitudes of these observations were $J \sim 22.0$ and $K \sim 20.6$.

In the HDF we make use of panoramic *K*-band imaging obtained by K. Bundy et al. (2004, in preparation) using WIRC2, as well as new *J*-band observations with the same instrument. The acquisition and reduction of the *K*-band data are described by K. Bundy et al. (2004, in preparation). The observations comprise three 8.′5 × 8.′5 pointings completely covering the GOODS HDF-N axis with per pointing exposure times of 15 ks and seeing of 0.″9 in *K*. We automatically aligned and mosaicked these images using STARLINK CCDPACK routines and combined them with the publicly accessible *HK* image provided by Capak et al. (2004) after suitable normalization. The *J*-band imaging for this field was obtained on 2004 January 6–7 with WIRC2, under nonphotometric conditions and with 1.″5 seeing. Three pointings were obtained that cover the bulk of

TABLE 1
PHOTOMETRY OF SMGS AND OFRGS

ID	z	K	J	I	Comment
SMM J030252.50+000856.4	0.176	16.15 ± 0.01	17.58 ± 0.02	20.80 ± 0.03	CFRS 03.10
SMM J030236.15+000817.1	2.435	≥20.9	≥21.3	≥23.7	CFRS 03.6
SMM J030227.73+000653.5	1.407	19.14 ± 0.03	19.66 ± 0.04	21.29 ± 0.05	CFRS 03.15
SMM J030231.81+001031.3	1.316	≥20.9	...	≥23.7	CFRS 03.17
SMM J030238.62+001106.3	0.276	20.52 ± 0.17	...	23.14 ± 0.17	CFRS 03.25
SMM J105238.30+572435.8	3.036	20.32 ± 0.24	...	23.26 ± 0.16	LH 850.2
SMM J105158.02+571800.3	2.239	18.86 ± 0.09	...	23.24 ± 0.15	LH 850.3
SMM J105230.73+572209.5[a]	2.611	19.22 ± 0.16	...	22.71 ± 0.07	LH 850.6
SMM J105200.26+572421.7[a]	0.689	18.82 ± 0.09	...	21.59 ± 0.03	LH 850.8
SMM J105207.49+571904.0[a]	2.694	≥20.6	...	22.66 ± 0.08	LH 850.12

NOTE.—Table 1 is published in its entirety in the electronic edition of the *Astrophysical Journal*. A portion is shown here for guidance regarding its form and content.
[a] Photometry may be contaminated by near neighbor.

the SMG/OFRGs in this region, each with a total integration time of 11.6 ks in J. Again the observations were mosaicked using STARLINK CCDPACK. The zero points of both the J and K-band images are transformed onto the 2MASS photometric system and yield 3 σ limits in our 4″ photometric aperture of $J \sim 22.5$ and $K \sim 21.0$.

In addition to the WIRC2 observation listed above, we also obtained pointed high-resolution J- and K-band imaging of selected SMG/OFRGs from the United Kingdom Infrared Telescope (UKIRT). These observations cover targets in the CFRS 03, SA 13, and SA 22 fields and were obtained on the nights of 2003 February 26 and August 27–31 and in queue observing on the nights of 2003 September 8–9, 16–17, and 28 using the UFTI near-infrared imager or the UIST near-infrared imaging spectrograph. The typical exposure times are 4.8 ks in J and 3.2 ks in K with 0.″5–0.″6 seeing and resulting 3 σ limiting magnitudes for point sources of $J = 22.5$ and $K = 20.8$.

Finally, we obtained J- and K-band imaging of the SA 22 field using IRIS2 on the Anglo-Australian Telescope (AAT; Tinney et al. 2004). These observations were kindly undertaken by M. Sullivan on the nights of 2003 September 7–9. These data consist of 7.2 ks in J and 3.6 ks in K covering a 7.′7 × 7.′7 field in 1.″5–1.″9 seeing and provide 3 σ limits of $J = 21.0$ and $K = 20.3$.

All the observations employ multiple short exposures (sometimes co-added on-chip) on a dithered grid to construct a running sky flat, which along with suitable dark exposures is used to remove instrumental and sky structure from the final images. Typical per-frame exposure times were 4 × 30 s in K and 2 × 60 s in the J band for the Palomar observations, 90 s in K and 120 s in J for UKIRT, and 3 × 60 s in J and 60 s in the K band on the AAT. The Palomar observations were reduced in a standard manner with custom-written IRAF scripts, while the UKIRT and AAT observations were reprocessed with the relevant ORAC-DR pipelines.

For our optical coverage we use the published I-band photometry from Ivison et al. (2002) in the Lockman and ELAIS-N2 fields, while I-band imaging for the HDF comes from the Suprimecam images published by Capak et al. (2004). The SA 13 optical images are also taken with Suprimecam and were retrieved from the Subaru archive and reduced with the NEKOSOFT software pipeline (Yagi 1998). We also employ I-band imaging of SA 22, CFRS 03, and CFRS 14 taken with the LFC camera on the Palomar Hale 5 m telescope and reduced with the IRAF MSCRED package. Calibration in all cases comes from observations of Landolt (1992) standard stars. Astrometry of all of the optical (and near-infrared) imaging was tied to the USNO catalog using interactive fits within the STARLINK GAIA tool. These astrometric solutions provide ≲0.″5 rms fits to the positions of the USNO stars in all frames.

We measure 4″ diameter aperture magnitudes for all the SMGs and OFRGs from Chapman et al. (2003a, 2004a, 2004b) lying within our *IJK* imaging after correcting for significant seeing differences between the passbands. We use this photometry to provide both *total* colors and magnitudes for the galaxies and list the latter in Table 1, along with the source ID, redshifts from Chapman et al. (2003a, 2004a, 2004b), and any identifiers from previous studies. The apertures were centered on the positions of the radio sources but were allowed to shift by up to 1″ to reflect the possible positional mismatch between the optical/near-infrared and radio astrometry in each field.

We illustrate the distribution of the SMG/OFRG sample on the $(I - K)$–K and $(J - K)$–K color-magnitude planes in Figure 1 and contrast this with the color-magnitude distribution of the general field galaxy population taken from a K-selected survey in the HDF-N (K. Bundy et al. 2004, in preparation). In Figure 2 we show a similar comparison of the $(J - K)$–$(I - K)$ color-color plane for the SMG/OFRGs and the field population.

2.2. *HST Optical Observations*

In addition to the ground-based imaging discussed above, we have also included in our analysis morphological information from higher resolution imaging of a subset of our sample from the *Hubble Space Telescope* (*HST*). This comprises multicolor ACS imaging of 20 galaxies from the spectroscopic SMG and OFRG samples of Chapman et al. (2003a, 2004a, 2004b) that serendipitously fall within the GOODS HDF-N field.

The five-epoch GOODS ACS F435W (B), F606W (V), and F775W (I) images were downloaded from the ST-ECF mirror of the GOODS web site. More details of the acquisition and reduction of these data are given in Giavalisco et al. (2004). We extract 7.″5 × 7.″5 regions centered on the 20 SMGs and OFRGs lying within the GOODS HDF-N imaging. We rebin these images to a scale of 0.″15 pixel^{-1} and then convolve them with a 0.″3 FWHM Gaussian to enhance low surface brightness features before constructing "true" color images, which are shown in Figure 3.

In total in the final sample we have 73 SMGs, 18 OFRGs, and five lensed SMGs, all with redshifts. For these we have K-band coverage of 89 galaxies, with J-band detections or

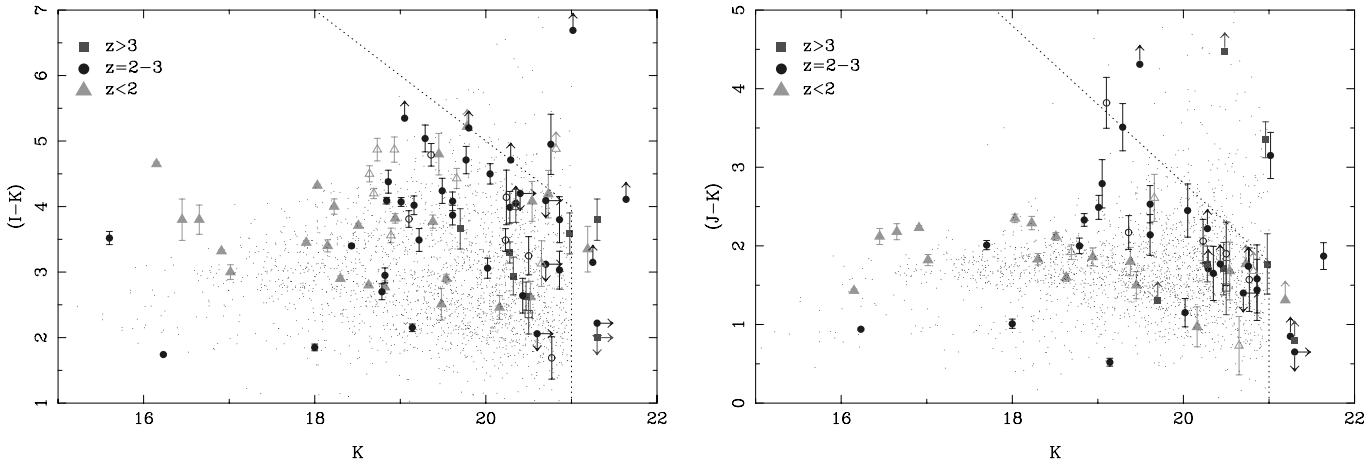

FIG. 1.—$(I-K)$–K and $(J-K)$–K color-magnitude diagrams for our sample of SMGs and OFRGs. The SMGs are plotted as filled symbols, and the OFRGs are plotted as open symbols, with all points coded on the galaxy redshifts. We also indicate representative 3 σ selection boundaries for the typical depth of our imaging. For comparison we also show the distribution of observed colors of the general population for a K-selected sample of galaxies in a 112 arcmin^2 region in the GOODS-North field (K. Bundy et al. 2004, in preparation). On average, the SMG/OFRG sample are redder than the typical field galaxies at their apparent magnitude: for example, at $K = 19-20$, the SMG/OFRGs have median colors of $(I-K) = 4.07 \pm 0.24$ and $(J-K) = 2.49 \pm 0.33$, whereas the general field colors are $(I-K) = 2.82 \pm 0.05$ and $(J-K) = 1.64 \pm 0.02$. [*See the electronic edition of the Journal for a color version of this figure.*]

limits for 63 of the galaxies in the combined sample. In addition, we have high-resolution *HST* imaging of 20 galaxies observed with ACS by GOODS.

The selection function for our combined sample is complicated, combining as it does submm, radio, optical photometric and spectroscopic, and near-infrared photometric selection limits. The easiest of these selection criteria to describe is that associated with the near-infrared imaging, which provides median 3 σ limits of $J \sim 22.5$ and $K \sim 20.9$.

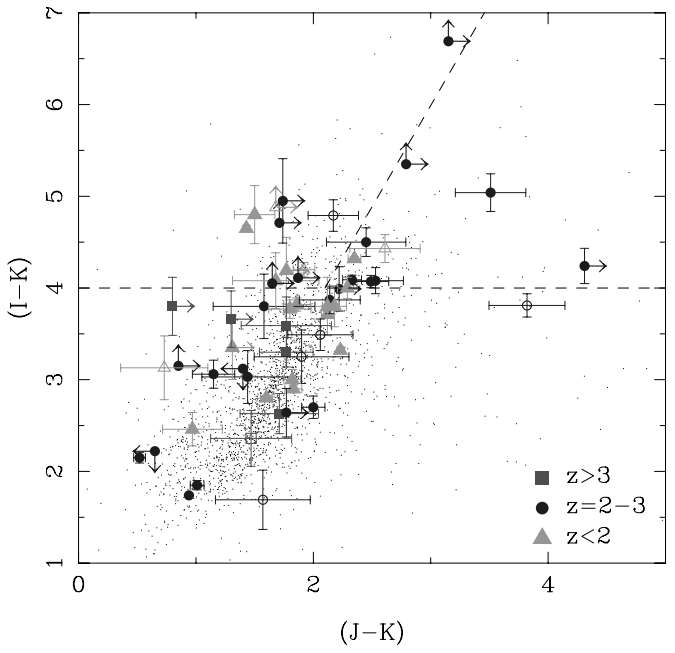

FIG. 2.—$(J-K)$–$(I-K)$ color-color plot for the SMG and OFRG galaxies in our spectroscopic sample and the lensed SMGs with redshifts from Frayer et al. (2004a). The OFRGs are plotted with open symbols, and all the points are coded in terms of their redshifts. We also indicate the classification scheme proposed by Bergstrom & Wiklind (2004) to distinguish between extremely red galaxies that are red by virtue of either dust [active star-forming galaxies with redder $(J-K)$ colors] or passive, evolved stellar populations [which have bluer $(J-K)$ colors] at $z < 2.2$. Note that this only applies to the SMG/OFRGs in our lowest redshift slice. Those SMG/OFRGs at $z < 2$ with $(I-K)$ colors sufficiently red to place them in the ERO class are roughly equally divided between these two photometric classes, underlining the difficulty of using simple schemes to attempt to disentangle the complex mix of obscured and unobscured activity within the most luminous galaxies at high z. [*See the electronic edition of the Journal for a color version of this figure.*]

The radio-selected SMG sample is defined by a minimum 850 μm flux of $\sim$5 mJy and a 1.4 GHz flux of greater than $\sim$30 μJy (Chapman et al. 2004a). Previous studies have shown that 60%–70% of a submm sample flux limited at 5 mJy is detectable above our radio flux limit (e.g., Ivison et al. 2002). The radio limit places a joint restriction on the highest redshift and coldest dust temperature for SMGs detectable in this survey. SMGs with characteristic dust temperatures around 40 K begin to fall below our radio flux limit at $z \gtrsim 3$, with colder SMGs missed at lower redshifts. The evolutionary models discussed by Chapman et al. (2004a) suggest that the radio-selected sample is likely to be 50% incomplete at $z \gtrsim 3$. As we are only considering SMGs with measured redshifts, we need to include the selection function from the spectroscopic identifications. Again, Chapman et al. (2004a) show that the bulk of the incompleteness in the spectroscopic follow-up (25% unidentified) likely arises from galaxies at $z \sim 1.3-1.8$, along with weak-lined, faint continuum sources over the full redshift range surveyed.

The OFRG sample from Chapman et al. (2004b) is defined by the absence of detectable 850 μm emission (2.5 σ limit of $<$5 mJy) from optically faint, apparently star-forming μJy radio sources ($R > 23.5$, $S_{1.4\,\mathrm{GHz}} \gtrsim 30$ μJy) at $z \gtrsim 1$. The star formation classification is based on their rest-frame UV spectral properties. At their redshifts the radio–far-infrared correlation implies that these galaxies will have bolometric luminosities of $\gtrsim 10^{12}\ L_\odot$. As Chapman et al. (2004b) discuss, the lack of detectable submm emission from these luminous galaxies is most likely explained by their hot characteristic dust temperatures (see also Blain et al. 2004b). The OFRGs thus likely complement the SMG population, sampling the properties of similarly far-infrared–luminous galaxies with somewhat hotter dust temperatures.

The combination of selection criteria means that we do not describe the sample as "complete" in any formal sense; rather, it is representative of the properties of a large fraction of the most far-infrared–luminous galaxies at $z \sim 1-3$. In particular,

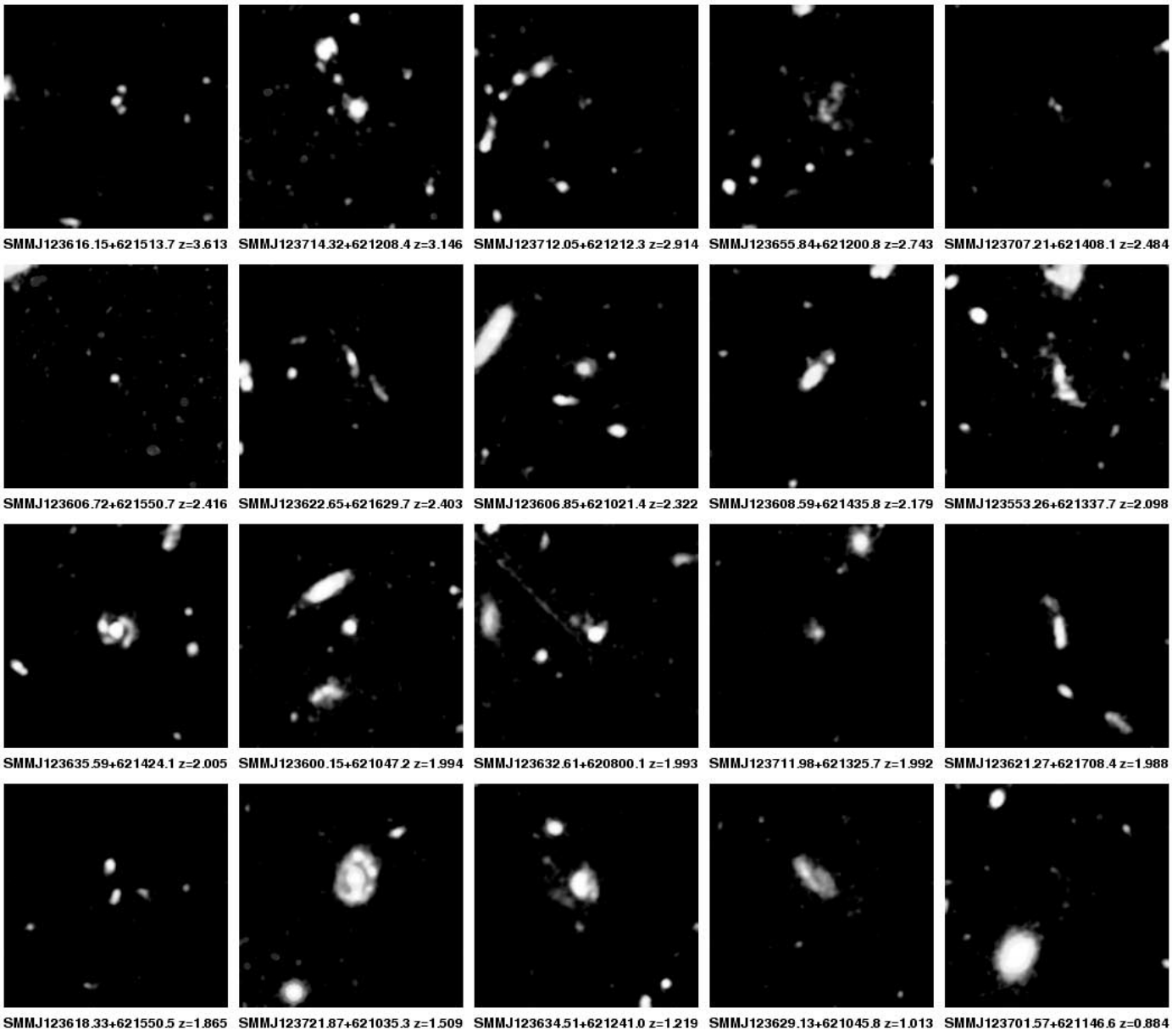

FIG. 3.—*BVI* true-color images of 20 SMGs and OFRGs in the GOODS/HDF-N region. These are ordered in terms of redshift (from $z = 3.6$ at the top left down to $z = 0.9$ at the bottom right). The following galaxies have $(I - K) \geq 4.0$: RG J123704.02, SMM J123712.05, SMM J123606.85, SMM J123707.21, SMM J123635.59, RG J123617.57, SMM J123621.27, RG J123640.74, RG J123623.54, SMM J123618.33, and SMM J123629.13. SMM J123616.15, SMM J123606.85, SMM J123606.72, and RG J123623.54 have bolometric luminosities exceeding $10^{13}\ L_{\odot}$. Each panel is 7″.5 square, centered on the spectroscopic source, and has north up and east to the left. [*See the electronic edition of the Journal for a color version of this figure.*]

we note that our sample is likely to be incomplete for the optically faintest SMG/OFRGs ($I \gtrsim 24.5$) because of our spectroscopic survey limit. This may include the reddest examples of the population brighter than our nominal near-infrared magnitude limit of $K \lesssim 21$. We attempt to quantify the possible biases from our selection criteria in the next section.

Before combining the three samples, we check for differences in their photometric properties, finding median K-band magnitudes of $\langle K \rangle = 19.70 \pm 0.24$ for the SMGs, 20.23 ± 0.43 for the OFRGs, and 18.79 ± 1.28 for the lensed SMGs (corrected to the source plane). Similarly, the median $\langle (I - K) \rangle = 3.71 \pm 0.16$ for the SMGs, 4.14 ± 0.30 for the OFRGs, and 4.00 ± 0.75 for the lensed SMGs, while the median $(J - K)$ colors are $\langle (J - K) \rangle = 1.73 \pm 0.10$, 1.91 ± 0.17, and 2.23 ± 0.26, respectively. Thus, the median properties differ by less than 2 σ for the three samples, so we feel that it is justifiable to combine the samples to study the photometric properties of luminous, dusty galaxies at high redshift. Nevertheless, we distinguish the OFRG and SMG samples in the plots so that the reader can judge the behavior of the separate populations. The combined sample has $\langle K \rangle = 19.70 \pm 0.23$, $\langle (I - K) \rangle = 3.80 \pm 0.13$, and $\langle (J - K) \rangle = 1.77 \pm 0.06$. Removing all those galaxies that could be affected by photometric contamination changes these median magnitudes/colors by less than 0.3 σ.

3. ANALYSIS AND RESULTS

3.1. *Color-Magnitude and Color-Color Distributions*

Our *IJK* photometry for 96 SMG/OFRGs (Table 1) with complete redshift information allows us to study the rest-frame

optical properties of a large sample of confirmed high-redshift dusty, luminous galaxies for the first time (cf. Smail et al. 2002b; Frayer et al. 2004a). We show the color-magnitude plots for the sample in Figure 1 and note that there is no strong trend of apparent color with redshift once the selection boundaries imposed by the depth of our available imaging are taken into account.

The primary selection criterion for inclusion in our sample is detectable submm/radio emission ($S_{850\,\mu m} \gtrsim 5$ mJy and/or $S_{1.4\,GHz} \gtrsim 30$ μJy). The only other major selection criteria that limit the characteristics of the galaxies we can study are those that affect the measurement of a redshift. As discussed above, there are two classes of SMG/OFRG for which it is more difficult to obtain spectroscopic redshifts, and hence they may be underrepresented in our sample: both galaxies at $z \sim 1.3$–1.8, from which no strong emission or absorption features fall in the sensitive range of the LRIS spectrograph; and galaxies without emission lines at very faint magnitudes, $I \gtrsim 24.5$ (see also Chapman et al. 2003a, 2004a).

To determine how these selection criteria may have affected the optical–near-infrared photometric properties of our sample, we begin by comparing the K-band magnitudes and $(I - K)$ colors of our spectroscopic sample (Fig. 1) with those for the counterparts of a flux-limited submm survey, which have been precisely located from their radio emission. This will highlight any biases that arise from our requirement for a spectroscopic redshift. Ivison et al. (2002) identify counterparts to submm sources with typical 850 μm fluxes of $\sim$8 mJy, and for those with robust radio IDs (which comprise $\gtrsim$60%–70% of the whole submm population at this depth) they find that the fraction of the population with $K \lesssim 21$ is 85%. Similarly, looking at the fraction of the population with unusually red colors, they find that 33% $\pm$ 14% are extremely red objects (EROs) with $(I - K) \geq 5.0$. This fraction rises to 55% $\pm$ 17% with $(I - K) \geq 4.0$, while only 6% are blank (defined as $I \geq 26$ and $K \geq 21$). In comparison, for our spectroscopic sample we find that 90% are detected with $K \lesssim 21$, 9% $\pm$ 3% of these have $(I - K) \geq 5.0$, and 43% $\pm$ 7% have $(I - K) \geq 4.0$. These contrast with fractions of 3% and 12%, respectively, seen in the general $K < 21$ field population at the same median K magnitude. Thus, we have a lower fraction of the very reddest galaxies, but we appear to fairly sample those SMGs with $(I - K) \lesssim 5$. We conclude that our spectroscopic sample of SMGs is broadly representative of the whole radio-identified submm population.

Comparing our $(I - K)$ colors with those measured for the counterparts in a purely submm flux–limited sample is much more uncertain because in the absence of either a radio or an ERO counterpart it is difficult for such surveys to reliably identify the correct counterpart. Webb et al. (2003) show that 40% $\pm$ 15% of their *secure* sample in the CFRS 03 and CFRS 14 (which includes SMGs both with and without radio counterparts) have $(I - K) \geq 4.0$ [and 5% $\pm$ 5% have $(I - K) \geq 5.0$]. In comparison, Ivison et al. (2002) quote a fraction of $(I - K) \geq 5.0$ ERO counterparts of 22%–27% in their full submm catalog, with between 6% and 43% blank.[5] Hence, we conclude that if our sample is biased against optical/near-infrared–faint counterparts, then this bias is no worse than for a radio-identified sample.

There are two published analyses of the near-infrared colors of SMGs (Fig. 1): Frayer et al. (2004a) and Dannerbauer et al. (2004). These studies provide *JK* photometry on small samples of lensed SMGs and radio/millimeter-identified MAMBO sources. We combine these two small samples and determine a median color of $(J - K) = 2.1 \pm 0.2$, with 23% $\pm$ 10% having $(J - K) \geq 3.0$ and $K \lesssim 22.5$, and 41% $\pm$ 14% having $(J - K) \geq 2.3$. This compares with just 7% $\pm$ 3% (4/61) with $(J - K) \geq 3.0$ and 18% $\pm$ 5% (11/61) with $(J - K) \geq 2.3$ in our spectroscopic sample (and 8% and 15%, respectively, for the $K < 21$ field population). The spectroscopic sample thus tends to be bluer than this faint, approximately flux-limited submm sample, although the small size of the latter means these differences are not significant.

We can also use our near-infrared imaging to determine whether we could select the counterparts to the SMG/OFRGs in our sample, *without* the need for detectable radio emission. We find that our SMG/OFRGs are either the brightest K-band source within an 8″ diameter region around their position (a typical error box for a submm source) or, if not the brightest, then typically the reddest galaxy in $(I - K)$ (Webb et al. 2003; Borys et al. 2004). For example, of the 25 SMG/OFRGs in the GOODS HDF-N field, 16 are associated with the brightest K-band galaxy within 8″, while the remaining nine are on average 0.27 ± 0.70 mag redder in $(I - K)$ than any equally bright or brighter companions (with only 3/25, or 12%, being bluer). We caution that our spectroscopic sample will tend to have brighter counterparts (in all bands) than a purely submm-selected sample. Hence, unfortunately, this approach does not provide an unambiguous identification of the true counterparts to complete samples of submm sources. Moreover, as we show below, the counterparts across our sample already span more than 6 mag in their K-band brightness—hence, the identity of the true counterpart will always remain ambiguous. In part, this reflects the fact that the K-band emission from these galaxies is only weakly coupled to their far-infrared emission, in contrast to their radio emission, which arises from a closely related process. Recent mid-infrared observations from *Spitzer* suggest that this may also prove to be a useful waveband for obtaining complete identifications of counterparts to submm/mm sources (Ivison et al. 2004; Egami et al. 2004).

The distribution of our SMG/OFRG sample on the $(I - K)$–$(J - K)$ color-color plane (Fig. 2) follows the same color-color distribution as the general field population, with a tendency for redder colors in both $(I - K)$ and $(J - K)$. Such color-color plots have been discussed as a tool to distinguish different classes of EROs (Pozzetti & Mannucci 2000; Bergstrom & Wiklind 2004) and have been tested with submm- and radio-selected samples (Webb et al. 2003; Dannerbauer et al. 2004; Smail et al. 2002a). The proposed classification boundary between the passive and dusty populations appears to split the current sample, rather than confining it to the dusty side of the classification region. As our SMG/OFRG sample are selected to be far-infrared–luminous systems, it seems unlikely that their *IJK* colors are dominated by old, passive stellar populations. Rather, we view this failure as an indication that simple two-color classification schemes may be ineffective for isolating dusty EROs because of the complex mix of obscured and unobscured emission in these systems. We emphasize that this failure persists when we isolate only those SMG/OFRG EROs at $z < 2$ (cf. Bergstrom & Wiklind 2004). We also reiterate that only a modest fraction of SMG/OFRGs have red enough colors, $\sim$10%–30% with $(I - K) \geq 5.0$, to be judged to be unusual (Smail et al. 1999a; Webb et al. 2004), and hence this type of classification scheme is only of limited use for the SMG/OFRG population.

[5] Note that it has been suggested that a fraction of the radio-blank submm sources may be spurious (Greve et al. 2004a).

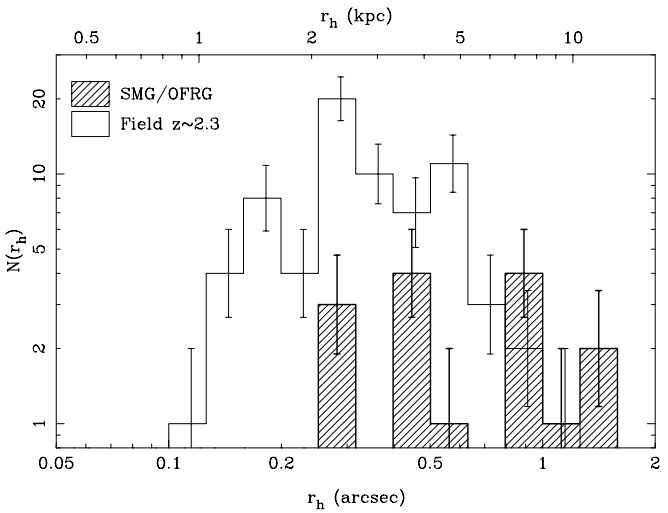

FIG. 4.—Comparison of the half-light distribution for the SMG/OFRG sample at $z = 1.8$–3.0 lying in the GOODS field with the distribution for the optically selected galaxy population at a comparable redshift, $z \sim 2.3$, from Ferguson et al. (2004). The top axis shows the actual scale sizes adopting an average angular scale of 8.3 kpc arcsec^{-1}. The SMG/OFRG sample clearly have much larger UV extents than a typical galaxy selected at these redshifts from a magnitude-limited sample.

3.2. *Morphological Properties*

We show true-color representations of 20 galaxies from our sample that lie within the GOODS-N field in Figure 3. These are derived from the *HST* ACS *BVI* images of this field. This sample spans $z = 1.0$–3.6 and contains 11 SMG/OFRGs with $(I - K) \geq 4.0$ but no galaxies with $(I - K) \geq 5.0$: SMM J123712.05 with $(I - K) = 4.95 \pm 0.45$ and RG J123640.74 with $(I - K) \geq 4.88$ are the reddest in the sample. Four of these systems have estimated bolometric luminosities in excess of $\geq 10^{13}\ L_{\odot}$.

We can use the high-resolution optical imaging to classify the morphologies of these reliably identified dusty galaxies and contrast these with conclusions from similar studies with much less robust counterparts (e.g., Smail et al. 1998). We find that just over half the sample (50%–60%) are apparently multicomponent or disturbed systems, suggestive of mergers or interactions. However, we caution that the presence of highly structured dust within these galaxies might mimic such structural peculiarities (see Fig. 4 and also Smail et al. 1999b). Twenty-five percent of the remaining SMG/OFRG are peculiar, including two face-on spirals, one of which has a ring; and only 15% are regular/normal. Of the apparently multicomponent systems, half contain at least one component that is an obvious disk galaxy.

The median angular scale of these galaxies is $\sim$8.4 kpc arcsec^{-1}, and it varies by only $\pm$5% over their redshift range, from 8.2 kpc arcsec^{-1} at $z = 1.0$ up to 8.5 kpc arcsec^{-1} at $z \sim 2$ and then dropping back to 7.4 kpc arcsec^{-1} at $z = 3.6$. Hence, the changing apparent size of these galaxies reflects either variations in their true physical extents or surface brightness dimming. There is clearly a trend for smaller systems at higher redshifts; however, the scatter at a fixed redshift is at least as large as the variation due to this trend. The median apparent size of the whole sample is $2\farcs3 \pm 0\farcs9$, measured at a fixed isophote (2.5 σ of the sky) along the major axis of the objects in the combined $B + V + I$ images. Using their redshifts, we calculate that this corresponds to an average physical size of 27 ± 17 kpc. We also measure the half-light radii of the SMGs in an analogous manner to that used by Ferguson et al. (2004), on the same *HST* data, and compare these with their distribution for the general optically selected population at $z \sim 2.3$ (using the 15 galaxies in our sample with $z = 1.9$–3, giving a similar average redshift for the subsample). We show this comparison in Figure 4, which demonstrates that the average SMG/OFRG in our sample at $z \sim 2.2$ is roughly twice as large as a typical optically selected galaxy from a similar magnitude-limited sample at this epoch.

Our results on the morphologies and sizes of the submm population echo those of Chapman et al. (2003b), who concluded from their sample of 13 submm-selected galaxies with STIS or WFPC2 imaging that 83% have irregular morphologies and just 17% had regular structure (this is almost identical to the 85% $\pm$ 10% and 15% $\pm$ 2% for our sample). Chapman et al. (2003b) also compared the UV sizes of their SMGs with samples of Lyman-break galaxies (LBGs) and magnitude-matched optically selected galaxies and suggested that the SMGs were larger than either of these comparison samples. The availability of redshifts for our sample has allowed us to demonstrate that these dusty, luminous systems are on average twice as large as the typical galaxy at their epoch.

We have also compared the observed *K*-band and optical morphologies of all the galaxies in the GOODS HDF-N region to search for more obscured components within these systems. We find that $\sim$20% (3/18) of the sample display near-infrared morphologies that strongly deviate from those seen in the optical. We show these three galaxies in Figure 5, where we see that there are extremely red components within some of these systems, with $(I - K) \geq 5$, on scales from 5 to 20 kpc. We also find evidence for dust extinction within some of the systems, which may help to explain the apparently disturbed, multicomponent structures of these galaxies. The near-infrared morphologies of some of our SMG/OFRGs show strong similarities to those of high-redshift luminous radio galaxies (Pentericci et al. 2001), hinting at a similar mode of triggering for the activity in these two populations. The presence of very red components on $\sim 2''$ scales within some SMG/OFRGs underlines the need for large-aperture photometry to derive reliable colors for the whole system (cf. Dannerbauer et al. 2004). We will discuss the internal structure of the SMGs on less than 1 kpc scales in a future paper using a sample of *HST* NICMOS and ACS imaging of galaxies from our spectroscopic SMG/OFRG sample.

3.3. *Magnitude-Redshift and Color-Redshift Distributions*

We now begin to investigate the variation of galaxy properties with redshift within our sample. We show in Figure 6 the *K*-band Hubble diagram for our sample of dusty, luminous galaxies and compare this with the behavior of local and more distant ULIRGs, as well as samples of powerful, high-redshift radio galaxies.

We note that we see no trend of *K*-band magnitude with $S_{850\,\mu\mathrm{m}}$ within the SMG/OFRG sample. This is at odds with Smail et al. (2002a), who suggested that galaxies that were fainter submm sources might also be fainter in the *K* band (but see Webb et al. 2003). However, we caution that our current sample is restricted in the brightness of the counterparts by the need to measure a spectroscopic redshift and hence is not ideal for performing this test. In particular, the 5 mJy submm flux limit for our SMG sample means that we have only marginal overlap with the flux regime studied by Smail et al. (2002a).

Turning back to the *K*-*z* relation in Figure 6 and discarding the two bright *K*-band counterparts that are obvious broad-line

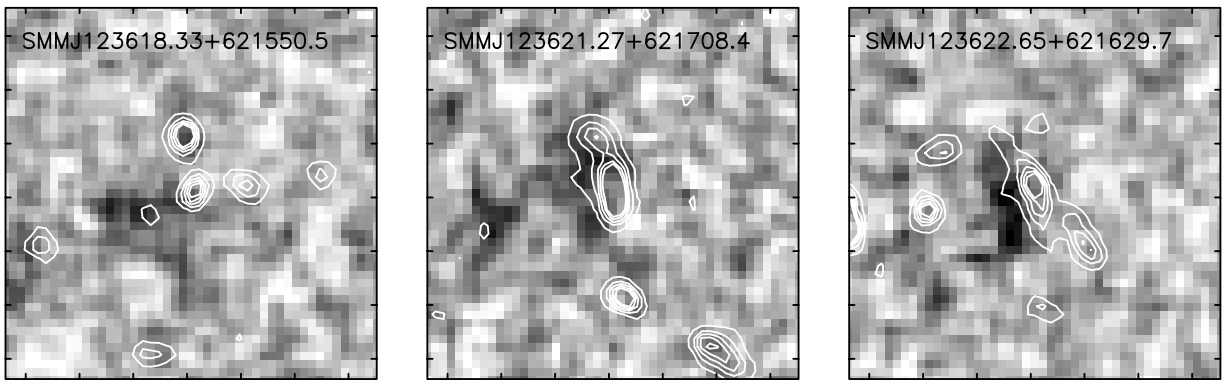

FIG. 5.—*K*-band images, shown as a gray scale, and the combined *BVI HST* images (*contours*) for three SMGs from the GOODS ACS region where the two wavebands show very different structures. In SMM J123618.33 the *K*-band light arises from an extremely red component $\sim$1″.5–2″ ($\sim$15 kpc) to the east of our optically identified counterpart. Similarly, in SMM J123622.65 the near-infrared emission lies on the edge of the optical extent of the galaxy, corresponding to a projected offset of $\sim$5 kpc. In SMM J123621.27, the peak in the *K*-band light within the galaxy lies in a saddle between two optically bright components, while a second extremely red source is $\sim$2″.5 ($\sim$20 kpc) to the east. Each panel is 7″.5 × 7″.5, and as the galaxies are all close to $z \sim 2$, this corresponds to $\sim$65 kpc. The contours are linearly spaced with an increment of 5 σ of the sky noise. The optical and near-infrared images have been smoothed with 0″.3 and 0″.5 FWHM Gaussians, respectively, to enhance the contrast in the relevant structures. The images in each passband are locally aligned using bright, compact galaxies and have a typical error in the alignment of less than 0″.2.

AGNs, we see that the bright wing of the SMG/OFRG distribution matches that traced by high-redshift luminous radio galaxies, roughly corresponding to $\sim 5L^*$. However, in contrast to the tight radio galaxy distribution, the SMG/OFRG sample spans a 4–5 mag range in *K*-band brightness at a fixed redshift and roughly tracks the predicted locus of an unevolving $3L^*$ elliptical galaxy. The large variation in the *K*-band magnitudes of SMG/OFRGs is perhaps unsurprising given that many of these galaxies appear to be multicomponent systems, with strong internal extinction and young starburst ages (Smail et al. 2003a).

We fit a simple polynomial relation to the variation of *K*-band apparent magnitude with redshift for the SMG/OFRG sample (having removed the two obvious luminous $K \sim 16$ AGNs at $z > 2$) and derive a best-fit relation of $K = 18.51 + 2.90[\log_{10}(z)] + 2.396[\log_{10}(z)]^2$ with a scatter of $\sigma_K = 0.97$ mag around this.[6] This scatter is 60% higher than that seen in the luminous radio galaxy population at similar redshifts (Willott et al. 2003). The SMG/OFRG sample also shows an offset of $\Delta K = 0.95 \pm 0.19$ from the radio galaxy *K*-*z* relation of Willott et al. (2003), indicating that the SMG/OFRGs are intrinsically less luminous in the rest-frame *V* band than powerful radio galaxies at the same redshift. Applying the reddening estimates from the photometric modeling (§ 3.5) reduces the scatter in the SMG/OFRG *K*-*z* relation by $\lesssim$10%–20%, although the fainter galaxies tend to be bluer in $(I - K)$ at a fixed *z* (Fig. 7) and so have lower estimated reddenings. Looking at the scatter around this fit for the 11 galaxies with bolometric luminosities of greater than $10^{13}\ L_\odot$ and *K*-band coverage, we find only a marginally smaller dispersion $\sigma_K = 0.90$ mag. If we fit the polynomial to just these 11 galaxies, the dispersion of the fit drops marginally to $\sigma_K = 0.74$ mag, but a Monte Carlo simulation indicates that this reduction in scatter is not statistically significant, with the fits for 17% of random samples of 11 SMG/OFRGs from our catalog showing dispersions below 0.74 mag (cf. Serjeant et al. 2003). A definitive conclusion about the tightness of the *K*-*z* relation for the most luminous galaxies will have to await a larger and more homogeneous sample than either of those used so far.

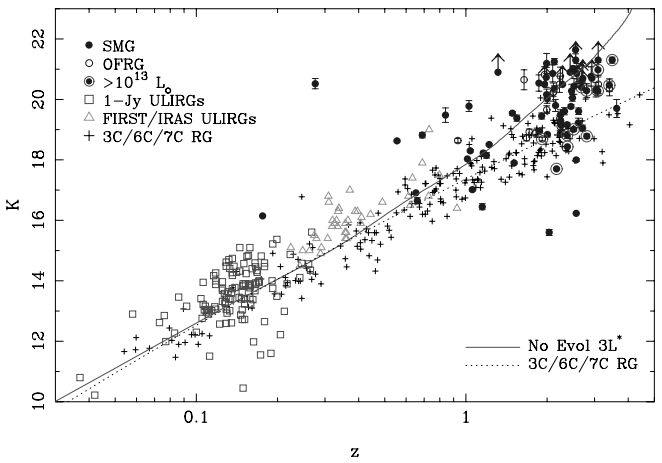

FIG. 6.—Variation of apparent *K*-band magnitude in a fixed 4″ ($\sim$34 kpc) diameter aperture with redshift for the SMGs and OFRGs in our sample. We also plot the *K*-band photometry of local ULIRGs from the 1 Jy sample of Kim et al. (2002) and for more distant greater than $10^{12}\ L_\odot$ systems from the sample of FIRST/*IRAS* galaxies of Stanford et al. (2000). In addition, we show the compilation of *K*-band photometry on powerful radio galaxies collected by Willott et al. (2003). Finally, we plot the expected variation with redshift for a nonevolving $3L_K^*$ galaxy (where $M_K^* = -24.3$; Kochanek et al. 2001) and the best-fit relation for the powerful radio galaxy sample from Willott et al. (2003). [*See the electronic edition of the Journal for a color version of this figure.*]

We can also invert the *K*-band Hubble diagram and ask how precisely we could estimate the redshift for an SMG/OFRG given an apparent *K*-band magnitude. We determine a simple linear relation with $z = -4.28 + 0.33K$ with $\Delta z/z = 0.41$ (again after discarding the two bright AGNs). Hence, near-infrared photometry provides only a very crude measure of the redshift for SMG/OFRGs.

Finally, we look at the variation in the optical–near-infrared colors of the sample with redshift. As Figure 7 shows, we find

[6] Removing those objects whose photometry may be contaminated by near neighbors does not significantly reduce the scatter in this fit. Similarly, removing SMM J030238.62+001106.3, the outlier at $z = 0.28/K \sim 20.5$, only reduces the scatter to $\sigma_K = 0.89$ mag. We believe that the redshift for this source probably refers to an unrelated foreground dwarf galaxy, with the true SMG counterpart being even fainter and at $z > 1$.

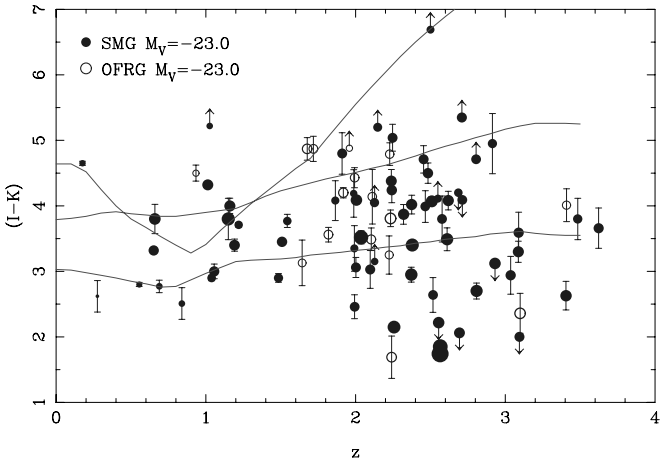

FIG. 7.—Distribution of SMG/OFRGs on the $(I-K)$–z plane. We compare this with the predicted $(I-K)$ colors as a function of redshift of three local ULIRGs derived from their observed rest-frame UV SEDs by Trentham et al. (1999). We see that there is a wide range in apparent colors of SMG/OFRGs at a fixed redshift, in line with that expected from the rest-frame UV colors of local ULIRGs. We believe that the diversity of colors probably reflects a wide range of internal obscuration and mix of components within these galaxies—the presence of multiple components and highly structured dust is also indicated by the UV and near-infrared morphologies of these galaxies (Figs. 3 and 5). We scale the size of each point with the reddening-corrected absolute V-band magnitude of the galaxy, assuming a constant SFR model. For completeness we note that there is no significant correlation of median colors with 850 μm flux and no correlation of 850 μm flux with redshift (Chapman et al. 2004a). [*See the electronic edition of the Journal for a color version of this figure.*]

no discernible trends in the median $\langle(I-K)\rangle$ (or $\langle(J-K)\rangle$) with z, with the gradients of fits to the median values of three bins with equal numbers of galaxies consistent with zero. The trends of color with redshift are roughly bracketed by the predicted tracks for three local ULIRGs from Trentham et al. (1999), once allowance is made for our likely incompleteness for the reddest galaxies (§ 3.1). However, there is a substantial fraction of the population that are even bluer in $(I-K)$ than the bluest of the three ULIRGs observed by Trentham et al. (1999), although this is hardly surprising given their small sample. We attribute the wide variation in rest-frame UV-optical colors of SMG/OFRGs to differing levels of obscuration and mixes of unobscured and obscured components within the galaxies. In part, this variety may come about as a result of different ages for the activity within the systems, with systems becoming less obscured as they age, or by differences in the porosity of the obscuring material brought about through the actions of winds and outflows. Less obscured channels would provide an essential conduit for the escape of the Lyα emission frequently identified in the spectra of this purportedly dusty population (Chapman et al. 2003a, 2004a, 2004b).

3.4. *Comparison with Other High-z Populations*

Recently, a number of studies have been published dealing with the $(J-K)$ colors of faint field galaxies. A central claim of this work is that photometric selection in this color, specifically $(J-K)\geq 2.3$, is a reliable a route to identify galaxies at $z\gtrsim 2$ (Franx et al. 2003; Daddi et al. 2003). The $\sim$20% (11/61) of the SMG/OFRGs with $(J-K)\geq 2.3$ in our sample have median properties of $K=19.29\pm0.22$ and $z=2.25\pm0.15$, with one example at $z=1.01$ and the remaining 10 at $z=1.99$–2.62. This confirms that, at least for these dusty, active galaxies, a cut at $(J-K)\geq 2.3$ can cleanly select high-z counterparts to SMG/OFRGs. For comparison, a $(J-K)\geq 2.0$ selection leads to 30% of the sample at $z\lesssim 1.0$–1.5.

To estimate how large a fraction of the photometrically selected $(J-K)\geq 2.3$ population consists of SMG/OFRGs, we first estimate the median submm flux for this subsample, finding $S_{850\ \mu\mathrm{m}}=4.7\pm1.0$ mJy. Submm sources with this flux density have a corresponding surface density of $\sim$0.5 arcmin^{-2}, and hence the spectroscopic $(J-K)\geq 2.3$ fraction in our sample has an effective surface density of $\geq$0.1 arcmin^{-2}, representing only about 6% of the overall $(J-K)\geq 2.3$ population with $K<20.5$. The proportion of submm-bright $(J-K)\geq 2.3$ galaxies may correspond to at most 10% of this photometric class, suggesting that the overlap between the photometrically selected sample and SMG/OFRGs is at best modest (see also Dannerbauer et al. 2004). A similar analysis of UV-selected high-redshift samples by Chapman et al. (2000) confirms that extreme near-infrared colors do not appear to isolate the far-infrared–luminous fraction of the high-redshift galaxy population. However, given their apparently large stellar masses (and strong clustering; Daddi et al. 2003), it seems likely that the passive and recently star-forming galaxies with very red near-infrared colors at $z\sim2$ could be immediate descendants of the short-lived $z>2.5$ SMG/OFRG population.

We can also compare the photometric properties of our SMG/OFRG sample with samples of UV-selected star-forming galaxies identified at similar redshifts: the LBGs. For a sample of 18 SMG/OFRGs cut in redshift to match the redshift distribution and median redshift of LBGs in Shapley et al. (2001), $z=2.6$–3.4, we find $\langle K\rangle=20.49\pm0.20$, $\langle(I-K)\rangle=3.54\pm0.38$, and $\langle(J-K)\rangle=1.73\pm0.11$. By comparison, Shapley et al. (2001) LBGs have $\langle K\rangle=21.35\pm0.14$ ($N=42$), $\langle(I-K)\rangle=2.40\pm0.10$ after transforming from $(R_{\mathrm{AB}}-K)$ using $(R_{\mathrm{AB}}-I)\sim0.4$ appropriate for galaxies with their observed $(R_{\mathrm{AB}}-K)$ colors at $z>2.6$, and $\langle(J-K)\rangle=1.63\pm0.10$. Hence, the SMG/OFRGs lying within the redshift range of the classical LBG selection are typically twice as bright in the K band (rest-frame V band) and slightly redder in their rest-frame UV and optical colors. However, we note that our radio-selected sample would be incomplete for the faintest SMGs if there is a strong correlation between K-band and radio luminosities, leading to the detected SMGs being brighter, but bluer, than would be seen in a pure submm-selected sample.

The classical LBG samples lie at somewhat higher redshifts than the majority of our SMG/OFRG sample (this may in part be responsible for the poor overlap between these two populations; Chapman et al. 2000). Recent work by Steidel et al. (2004) has extended their photometric selection techniques to lower redshifts, $z=1.4$–2.6, giving a better match for comparison with the bulk of the SMG/OFRG population. These "BX/BM" samples (mean $z=2.23\pm0.31$) are brighter and redder than the LBG population: $\langle K\rangle=20.49\pm0.06$ (for $K<21$) and $\langle(I-K)\rangle=3.22\pm0.05$ [adopting $(R_{\mathrm{AB}}-I)\sim0.35$]. The equivalent measurements for the 57 SMGs/OFRGs at $z=1.4$–2.6 (mean $z=2.15\pm0.30$) in our sample are $\langle K\rangle=19.77\pm0.29$ and $\langle(I-K)\rangle=3.99\pm0.16$. Again, we find that the SMG/OFRGs are both brighter and redder than the UV-selected population at $z\sim2$. The difference in K-band magnitude amounts to roughly a factor of 2 difference between the typical rest-frame R-band luminosities of these two populations. Without more information it is impossible to determine whether this results from the larger stellar masses of the SMG/OFRG sample or from a strong contribution to their rest-frame R-band fluxes from the Hα line, which will fall in the observed K band at their typical redshifts. Swinbank et al.

(2004) discuss near-infrared spectroscopy of a sample of SMG/OFRGs and conclude that the Hα line typically contributes only about 10% of the broadband flux, so we suggest that the difference in mean K magnitude probably reflects the brighter continuum luminosity of the SMG/OFRG galaxies. Similarly, it is unlikely that emission-line contributions strongly skew the observed colors of the SMG/OFRGs, suggesting that the SMG/OFRGs have redder continua than the average BX/BM galaxy, although without more detailed modeling it is impossible to tell whether this is due to either more evolved stellar populations or dust reddening. Mid-infrared photometry of spectroscopically identified SMG/OFRGs from *Spitzer* should provide a powerful tool for distinguishing between these alternative explanations.

3.5. *Simple Photometric Modeling*

To try to constrain the extinction and ages of the activity in the SMG/OFRG population, we have sought to exploit the combination of broadband photometry and redshifts available for our sample. We start by simply plotting the rest-frame spectral energy distributions (SEDs) of the 46 galaxies with J- and K-band detections in Figure 8. If the galaxies have similar rest-frame SEDs, then their spread in redshift enables us to recover information about the SED shape on a finer scale than provided by the broadband colors. We have therefore also calculated the median rest-frame SED of this population and show this in Figure 8. The median SED shows a red continuum from $\sim$0.4 to 0.7 μm, with an apparent break to a steeper continuum slope below $\sim$0.4 μm. We compare this with the SED of an evolved stellar population and a young, highly reddened star-forming galaxy from STARBURST99 (Leitherer et al. 1999). The continuum slope in the red and the position of the break in the slope are both more consistent with the dusty, starburst model—with the discontinuity in the continuum slope arising from the Balmer break. However, we caution that the J band lies at $\sim$0.4 μm at the median redshift of our sample, and hence the strength of the apparent discontinuity might change if we included those galaxies with only limits on their J-band fluxes.

To provide a more quantitative analysis of the colors of SMG/OFRGs, we have fitted the observed *IJK* photometry of the galaxies at their observed redshifts using HYPER-Z (Bolzonella et al. 2000) to derive reddening estimates for the stellar populations in these systems, assuming that they are dominated by young starbursts (consistent with their intense far-infrared emission and the median SED derived above). For the underlying star formation histories we adopt either a single burst or constant star formation rate (SFR) model and a Calzetti reddening law with $A_V \leq 5.0$. We use a likelihood ratio test to select the best-fitting model at the known redshift, indicating that 66% are better fitted by the instantaneous burst models. We derive a mean age of the stellar populations in the $z > 1$ SMG/OFRG sample of 450 ± 80 Myr and a mean reddening of $A_V = 1.70 \pm 0.14$. This reddening is consistent with the range measured for the nuclear regions of local ULIRGs (Scoville et al. 2000). We also find, as expected, that the derived reddening correlates with $(I - K)$ at a fixed redshift and that the best-fit ages are greater at lower redshifts.

While the photometry for the majority of SMG/OFRGs is well fitted by these simple models, with 85% having probabilities for the fits of $\geq$95%, we caution that the constraints on individual galaxies are very weak, so in our discussion we focus on the ensemble properties of the sample (although we stress that the availability of precise redshifts removes much of the ambiguity in this analysis). We also note that the worst-fitting sources include several bright AGNs and that the galaxies with poorly fitted SEDs are uniformly distributed across the fields in our survey. To investigate the systematic errors in these estimates, we fit either just a single-burst model *or* a constant SFR model and derive mean ages and reddenings of 310 ± 90 Myr and $A_V = 1.70 \pm 0.14$ or 530 ± 80 Myr and $A_V = 2.44 \pm 0.13$, respectively. The relatively great ages for the single-burst model are inconsistent with the detection of strong far-infrared emission from star formation in these galaxies, so we interpret them rather as an indication of past star formation activity within these galaxies (on hundreds of Myr timescales). For this reason we prefer to use the reddenings and luminosities derived from the constant SFR model fits in the analysis that follows.

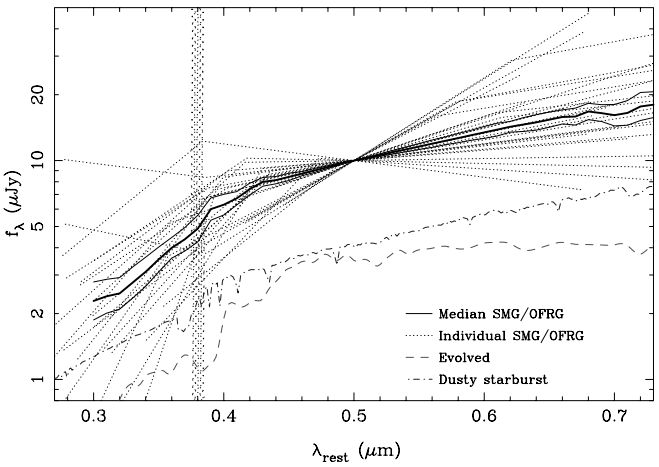

FIG. 8.—Rest-frame SEDs of those SMG/OFRGs that are detected in both the J and K bands (73% of those with J-band observations). These are arbitrarily normalized on the basis of their monochromatic flux at 0.5 μm. We show the SEDs of the individual galaxies and also the median of these as a function of wavelength, along with the 1 σ scatter on this estimate. The median SED shows a very red continuum shape with a discontinuity in the continuum slope around $\sim$0.4 μm. We compare this with two simple model SEDs: for an evolved stellar population, a luminous local elliptical galaxy; and a dusty starburst, based on a 100 Myr old constant SFR model with $A_V = 4$ from Leitherer et al. (1999). The dusty, young star-forming galaxy appears to provide a better match to the observed SED and suggests that the discontinuity in the continuum slope is associated with the Balmer break (*highlighted by the shaded region*). [*See the electronic edition of the Journal for a color version of this figure.*]

To attempt to compare the results of this modeling between populations, we have also applied this same fitting technique to the *RJK* photometry of the $z \sim 3$ LBGs in Shapley et al. (2001). Here we derive a mean age of 250 ± 80 Myr and a mean extinction of $A_V = 0.92 \pm 0.14$. Restricting ourselves to only a constant SFR model and requiring that the derived ages be in excess of 10 Myr, we measure a mean age of 330 ± 100 Myr and reddening of $E(B - V) = 0.32 \pm 0.05$, roughly consistent with the 590 ± 60 Myr and $E(B - V) = 0.17 \pm 0.01$ determined from a more careful analysis of their *GRJK* colors by Shapley et al. (2001). As we noted earlier, Steidel et al. (2004) have already shown that $z \sim 3$ LBGs are bluer/fainter in their rest frame than the $z \sim 2$ BX/BM population, so it would be informative to repeat this comparison when near-infrared photometry becomes available for the latter.

Given the uncertainties in this analysis and our limited data set, we conclude that the rest-frame UV/optical emission from the SMG/OFRG population is dominated by the light from a highly reddened and very young stellar population, with an age of just a few hundred Myr and typical continuum extinction

corresponding to a factor of $\gtrsim$50 times obscuration at 1500 Å. We estimate the reddening for the SMG/OFRGs to be at least twice that of the LBGs we have analyzed, and perhaps more, as a result of the degeneracy in the fits between greater ages and increased reddening. This indicates that the redder optical/near-infrared colors we measured in § 3.4 for the SMG/OFRG sample result from stronger extinction than that in the LBGs and BX/BM populations. Correcting for this stronger extinction would suggest that the SMG/OFRGs have dust-corrected, rest-frame optical luminosities at least 5 times brighter than typical BX/BM or LBG systems.

We can also test the consistency of the estimated ages and luminosities by determining whether it is possible to form the observed stellar population given the estimated SFR for the galaxies within the proposed timescale. We take the median V-band luminosity from the HYPER-Z SED fits and correct this on a case-by-case basis with the estimated reddening for each galaxy, giving us a median dereddened V-band luminosity of $L_V \sim 1.8\times10^{11}\ L_\odot$. For a system with a constant SFR and an age of a few hundred Myr we require an SFR of $\lesssim$1000 $M_\odot$ yr^{-1} (for stars more massive than 1 $M_\odot$) to build up this luminosity. The median far-infrared luminosity of the $z >$ 1 SMG/OFRG sample is $5\times10^{12}\ L_\odot$, corresponding to an SFR of $\sim2\times10^3\ M_\odot$ yr^{-1} for stars more massive than 1 $M_\odot$. This suggests that the star formation activity in the average SMG/OFRG, if it was maintained at the current level, is more than sufficient to produce the observed optical luminosities within the last 100 Myr. However, we feel that it is more likely that the activity is episodic, probably comprising short $\ll$100 Myr bursts spread over several hundred Myr. Such behavior would be consistent with that expected from merger-driven starbursts (Mihos & Hernquist 1996), as well as the apparent masses of black holes seen in some SMGs (Smail et al. 2003a, 2003b).

We can also use the estimated mass-to-light ratios of young starbursts derived using STARBURST99 (Leitherer et al. 1999) to estimate a minimum stellar mass for these systems: this gives an average mass-to-light ratio of $M/L_V \sim 0.15\ M_\odot/L_\odot$ for a system with either a constant SFR over a few hundred Myr or a $\lesssim$300 Myr starburst. Applying this to our reddening-corrected median V-band luminosity, we estimate that the typical SMG/OFRG contains $M_{\rm stars} \sim 3\times10^{10}\ M_\odot$ of young stars, in addition to any underlying older, more evolved population. Furthermore, millimeter-wave CO mapping of a handful of SMGs (Frayer et al. 1998, 1999; Neri et al. 2003) indicates that the median gas mass in submm-luminous galaxies is on the order of $M_{\rm gas} \sim 2\times10^{10}\ M_\odot$. This suggests that many of our SMG/OFRGs retain enough gas to continue forming stars at the current rate for a length of time similar to their current ages. Combining the stellar and gas masses gives a typical baryonic mass for an SMG in our sample of $M \sim 5\times10^{10}\ M_\odot$. This is comparable to the stellar mass of an L^* galaxy at the present day (Cole et al. 2001), indicating that over half our sample are likely to leave $\gtrsim L^*$ descendants at the present day (Genzel et al. 2003).

3.6. *Comparison with $z \ll 1$ ULIRGs*

There is a class of obscured, active galaxies at relatively low redshifts that have far-infrared luminosities almost comparable to those estimated for the SMG/OFRG population: the ULIRGs. If we can demonstrate that SMG/OFRGs share the same properties as ULIRGs, then we can use the much more detailed observational information available on the latter to infer more about the processes that may operate in the more distant population.

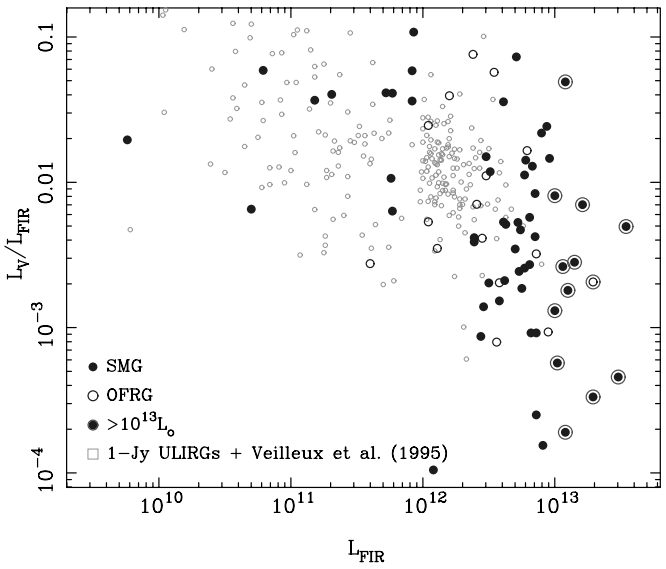

FIG. 9.—Ratio of rest-frame V-band luminosity to far-infrared luminosity as a function of far-infrared luminosity for the SMG/OFRG sample. We also show the distribution of the local ULIRGs in the 1 Jy ULIRG sample of Kim et al. (2002) and the luminous infrared galaxy sample of Veilleux et al. (1995), converted from M_R and M_B, respectively, to M_V using median colors of $(V-R) = 0.9$ and $(B-V) = 1.0$ corresponding to SEDs with their observed $(R-K)$ colors at $z \sim 0.15$. [*See the electronic edition of the Journal for a color version of this figure.*]

To compare the properties of the SMG/OFRG sample with similarly luminous low-redshift galaxies, we begin by using the rest-frame V-band luminosities from the photometric modeling described in the previous section. We stress that at the typical redshift of our SMG/OFRG sample the rest-frame V band is straddled by our observed JK photometry, making this estimate of their optical luminosities relatively straightforward. We plot the ratio of the V-band and far-infrared luminosities for our sample as a function of their far-infrared luminosities in Figure 9. We compare this distribution with the equivalent measurements for the samples of ULIRGs from Kim et al. (2002) and luminous infrared galaxies from Veilleux et al. (1995). For comparison, the median far-infrared luminosities are $(1.9 \pm 0.2)\times10^{12}\ L_\odot$ for the 1 Jy sample, converted to our cosmology; $(3.7 \pm 0.4)\times10^{12}\ L_\odot$ for $z = 1$–2.5 SMG/OFRGs; and $(5.0 \pm 0.6)\times10^{12}\ L_\odot$ for the full SMG/OFRG sample. Together, these samples exhibit a broad trend of lower $L_V/L_{\rm FIR}$ at higher luminosities, which has been interpreted as a signature of an increasing fraction of highly obscured star formation in more active systems (e.g., Serjeant et al. 2003).

As expected, the lower luminosity (usually lower redshift) systems within the SMG/OFRG sample are distributed within the broad correlation seen in the local far-infrared–selected samples, indicating that these galaxies are likely to be entirely analogous to similarly luminous, low-redshift systems selected from *IRAS* surveys.

The more typical, higher luminosity and higher redshift SMG/OFRGs extend the trends seen in the lower luminosity samples to lower $L_V/L_{\rm FIR}$ in more luminous galaxies, although with 2 orders of magnitude scatter at a fixed luminosity. To quantify the trend we see, we calculate the median $L_V/L_{\rm FIR}$ of the $z = 1$–2.5 SMG/OFRGs ($L_V/L_{\rm FIR} = 0.005 \pm 0.001$) and for the *IRAS* 1 Jy sample of Kim et al. (2002), $L_V/L_{\rm FIR} = 0.023 \pm 0.003$, showing that the SMG/OFRGs are roughly 4 times more obscured than local ULIRGs (Fig. 9).

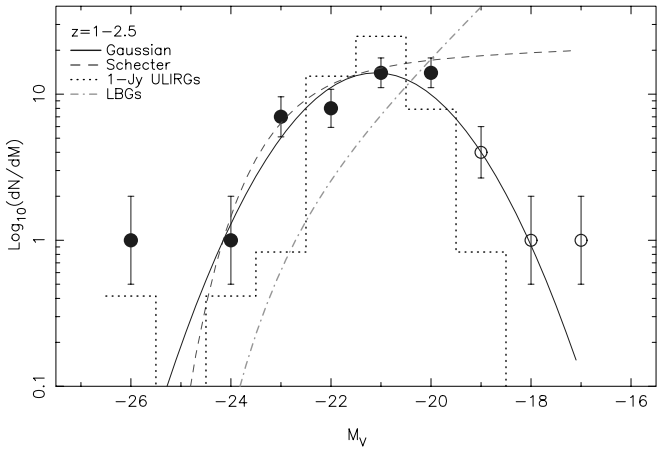

FIG. 10.—Absolute rest-frame *V*-band magnitudes of SMGs and OFRGs with redshifts lying in $z = 1-2.5$ (beyond which our *K*-band imaging becomes increasingly incomplete for counterparts with $M_V \lesssim -20$). We overplot fits to the $M_V \leq -20$ data points (*filled symbols*) for both Schecter and Gaussian function fits. For the Schechter function fit we derive $\alpha = -1.03 \pm 0.27$ and $M_V^* = -23.1 \pm 0.6$. From a Gaussian fit we estimate $\langle M_V \rangle = -21.1 \pm 0.25$ and $\sigma_V = 0.75 \pm 0.1$. We also show the rest-frame *V*-band luminosity function derived for $z \sim 3$ LBGs by Shapley et al. (2001) and that of local ULIRGs from the 1 Jy sample. These demonstrate that the typical SMG/OFRG has a rest-frame optical luminosity similar to that of ULIRGs at $z \sim 0$ (although it is several times brighter in the far-infrared) and has a characteristic luminosity that is 4 times brighter than the somewhat higher redshift LBG population (correcting for dust extinction will exacerbate this difference). [*See the electronic edition of the Journal for a color version of this figure.*]

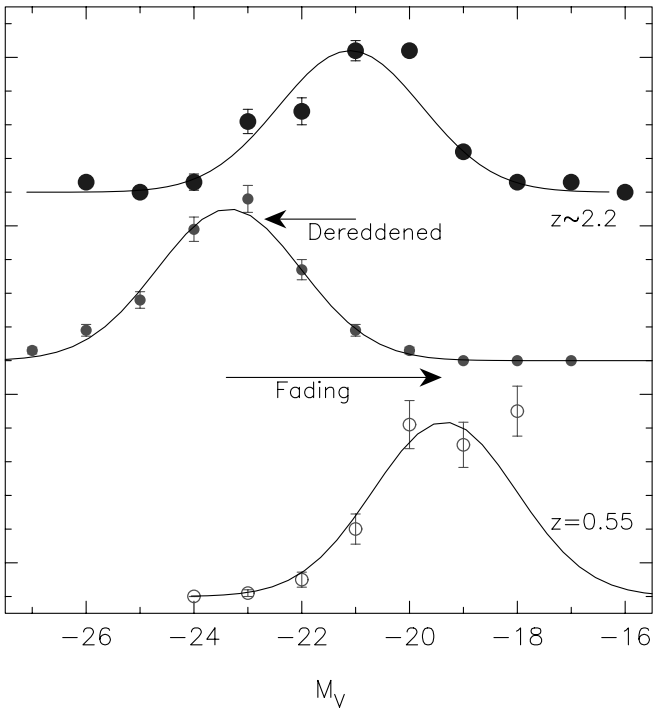

FIG. 11.—Observed rest-frame *V*-band luminosity function for the $z = 1-2.5$ SMG/OFRG sample along with a best-fit Gaussian function; the same distribution corrected for reddening using the individual extinction corrections estimated from the HYPER-Z fits to their *IJK* colors, also overlaid with its best-fit Gaussian function; and finally this same functional fit, after fading by $\Delta V \sim 4$ mag corresponding to passive evolution for 5.4 Gyr starting with a galaxy with a constant SFR history and an age of 100–500 Myr at $z = 2.2$. This predicted luminosity distribution is compared with the observed luminosity function of morphologically classified E/S0 galaxies in three $z \sim 0.55$ clusters from Ellis et al. (1997), adopting an arbitrary normalization. [*See the electronic edition of the Journal for a color version of this figure.*]

We have also used the rest-frame *V*-band absolute magnitudes for the SMG/OFRGs to construct a luminosity function for an approximately volume-limited sample of SMG/OFRGs brighter than $M_V = -20$ at $z = 1-2.5$. This is shown in Figure 10 and exhibits a steep rise at $M_V \gtrsim -24$, with a decline at $M_V \gtrsim -20$ that we attribute to incompleteness. We compare it with the equivalent distribution for the 1 Jy sample of local ULIRGs (Kim et al. 2002), which has a median absolute *V*-band magnitude of $M_V = -21.15 \pm 0.09$, converted from M_R using a typical color of $(V - R) = 0.9$ suitable for a galaxy SED at $z = 0.15$ with $(R - K) = 3.25$. The galaxies in the $z = 1-2.5$ SMG/OFRG sample have an almost identical median absolute magnitude: $M_V = -21.05 \pm 0.27$. Thus, the absolute *V*-band luminosities of the local ULIRGs and the distant SMG/OFRGs are very similar (Fig. 10), indicating that the factor of 4 difference in their $L_V/L_{\rm FIR}$ ratios (Fig. 9) is most likely due to the higher far-infrared luminosities of the distant galaxies. This is consistent with a constant star formation efficiency for low- and high-redshift starbursts (cf. Baugh et al. 2004), given the factor of 3 times higher gas fractions and larger gas masses seen in the distant SMG/OFRGs (Frayer et al. 1999; Neri et al. 2003).

3.7. *Evolution of SMGs*

As the final step in our analysis we wish to understand the evolution of SMG/OFRGs to the present day. To do this we take one extreme scenario and assume that the star formation activity we see is the last major event in these galaxies and that their subsequent evolution can be approximated by passive evolution. We can then employ simple stellar evolution models to predict the likely luminosity function of this population at lower redshifts and compare that with possible descendant populations. As we discussed in § 3.5, the large gas reservoirs detected in SMGs through their CO emission suggest that these galaxies retain enough gas to modestly increase their stellar masses. However, for the purposes of this simple discussion we ignore any additional sources of new stars.

To quantify our discussion, we use the characteristics of the $z > 1$ SMG/OFRG sample from our earlier analysis. We correct the rest-frame *V*-band luminosities of the galaxies using their individual estimates of A_V from the constant SFR fits and derive a reddening-corrected absolute magnitude of $M_V = -23.35 \pm 0.15$ for a sample with a median redshift of $z \sim 2.2$. The luminosity-weighted ages we derived from our HYPER-Z fits were a few hundred Myr, consistent with the expected ages of the starbursts in these massive galaxies from dynamical arguments. We now turn to the PEGASE spectral modeling package (Fioc & Rocca-Volmerange 1997) to estimate the rest-frame *V*-band fading of a system with a constant SFR for ~100–500 Myr (bracketing the likely range in ages), which is terminated at that point and is observed 5.3 Gyr later (corresponding to the time between $z \sim 2.2$ and 0.55). We find that the stellar populations are expected to fade by between $\Delta V = -3.5$ and -4.5 mag, so we take $\Delta V \sim -4$ as representative. Thus, the typical SMG/OFRG will have $M_V \sim -20$ at $z = 0.55$, assuming there are no subsequent star formation events.[7]

[7] We have chosen to undertake this comparison with $z = 0.55$ clusters because the passive galaxies populating the faint end of the luminosity function in more local clusters may be built up through a different process, involving passive fading or more active threshing/harassment of mid-/late-type disk galaxies accreted by the clusters since $z \sim 0.5-1$ (Dressler et al. 1997; de Lucia et al. 2004; Kodama et al. 2004). Hence, this comparison is most easily achieved with a distant cluster where the luminous elliptical population can be more easily isolated.

The proposed evolution of the luminosity function for SMG/OFRGs is illustrated in Figure 11. This shows the observed rest-frame *V*-band absolute magnitude distribution of the $z > 1$ SMG/OFRG sample, the same distribution corrected on an object-by-object basis for the estimated reddening, and then finally this distribution faded by 4 mag to represent the passive evolution from $z \sim 2.2$ to 0.55. The final distribution is compared with that of morphologically classified spheroidal galaxies (almost all of which are elliptical galaxies) in three $z \sim 0.55$ clusters from the study of Ellis et al. (1997; with arbitrary normalization). This comparison suggests that in this simple evolutionary picture the SMG/OFRG population can adequately match the bright end of the luminosity function of spheroidal galaxies seen in cluster environments. This is clearly highly speculative, but taken in conjunction with the large stellar masses we derive for these galaxies, their large dynamical masses (Swinbank et al. 2004; Neri et al. 2003; Greve et al. 2004b), and their strong clustering (Blain et al. 2004b), it provides circumstantial evidence for the association of the SMG/OFRGs with the early formation of the most luminous ($>L^*$) spheroidal galaxies.

4. DISCUSSION AND CONCLUSIONS

Our aim in this paper is to relate quantitatively the various populations of galaxies and AGNs now being uncovered in large numbers at $z \sim 2$. To give a qualitative indication of the form this relation might take, we note that one popular model for the creation of luminous, metal-rich elliptical galaxies has them formed through a short, intense, but highly obscured burst of star formation at high redshifts. Such activity would be naturally related to the SMG population (Lilly et al. 1999; Smail et al. 2002a). Similarly, the proposed presence of supermassive black holes in all luminous elliptical galaxies and the claimed correlation of their black hole masses with the stellar mass of their host spheroids argues that their progenitors are all likely to have exhibited some form of nuclear activity during their formation phase. Can we therefore use the space densities and likely lifetimes of the SMG, QSO, and elliptical galaxy populations to test a simple framework in which SMGs represent the monolithic formation of massive elliptical galaxies and evolve through a QSO phase (Sanders et al. 1988; Page et al. 2004)?

The volume density of bright SMGs is 3×10^{-5} Mpc^{-3} at $z \sim 2.5$ (Chapman et al. 2003a, 2004a). Including the submm-faint but similarly far-infrared–luminous OFRG population will roughly double this estimated space density. The combined population will then be about 10 times more numerous than optically selected QSOs with $M_B > -25$ at this epoch (Boyle et al. 2000). Similarly, luminous, evolved galaxies at $z \sim 1$ have a space density that is about 10 times higher than that of SMGs (Cimatti et al. 2002) and comparable to that of greater than L^* elliptical galaxies at $z \sim 0$. The redshift range covered by the bright SMG population corresponds to a time span of roughly 1–2 Gyr, suggesting that if individual SMGs are identified with luminous, evolved galaxies at $z \sim 1$ and greater than L^* elliptical galaxies at the present day, then individual SMGs must have lifetimes of only 100–200 Myr (see also Serjeant & Takagi 2004). We have shown earlier that this lifetime is sufficient to allow these galaxies to build up an L^* worth of stars, given the SFRs inferred from the far-infrared luminosities of bright SMGs ($\sim10^3\ M_\odot\ \mathrm{yr}^{-1}$). Indeed, the reddening-corrected, rest-frame *V*-band magnitudes of these galaxies imply that many already have substantial stellar masses (consistent with them being L^* galaxies). The ratio of SMG to QSO volume densities would then imply that the latter phase lasts around 10–20 Myr. This is then broadly consistent with independent estimates of the lifetime of bright QSOs (Martini & Weinberg 2001), as well as the relative ratio of submm-detected QSOs as a fraction of the QSO and SMG populations (Stevens et al. 2004; Chapman et al. 2004a).

Thus, we have a quantitatively self-consistent scenario. SMG/OFRGs are cumulative ~100–200 Myr long star formation events that build the stellar population of an $\gtrsim L^*$ elliptical galaxy at $z \sim 2-3$, before going through a ~10 Myr long QSO phase and then evolving to become the passive EROs seen at $z \sim 1$ [perhaps via a phase with $(J-K) \geq 2.3$ at $z \sim 2$; Cimatti et al. 2004] and subsequently the luminous elliptical population seen in intermediate and low-redshift clusters.

The alert reader will notice that there is no mention of the important UV-selected high-redshift galaxy populations in the framework outlined above. This is because we believe that there are strong reasons to expect that the typical UV-selected, star-forming galaxy at $z \sim 2-3$ is less massive than those identified through current far-infrared surveys. This belief is based in part on the differences in the rest-frame optical luminosities of the two populations we have uncovered. It is strengthened by the apparent differences in the dynamical mass estimates of small samples from the two populations (Swinbank et al. 2004; Erb et al. 2003) and from the strong clustering seen in the far-infrared–selected population (Blain et al. 2004b). All of these observations point toward SMG/OFRGs being several times more massive than typical UV-selected, high-redshift galaxies. Hence, it is unlikely that a typical UV-selected galaxy will experience a ULIRG-like phase in its evolution, although mergers of two such systems may produce sufficiently intense activity.

There are, however, problems with the simple evolutionary picture we have outlined. Not least of these are the suggestions that SMGs (and the very red near-infrared population at $z \sim 2$) are strongly clustered, with correlation lengths on the order of $\sim8\ h^{-1}$ Mpc (Blain et al. 2004b; Daddi et al. 2003). This is roughly twice that measured for typical QSOs at this epoch (although perhaps consistent with the brightest; see Croom et al. 2002). This may indicate that bright SMG/OFRGs do not evolve into typical QSOs or that a more complex temporal bias is operating (Scannapieco & Thacker 2003). More reliable clustering measurements will be needed for all populations before this becomes a critical issue, yet it does remain a concern.

A second test of this simple evolutionary picture will be provided from more reliable measurements of the stellar masses of the various populations. At $z \sim 2-3$ this requires sensitive mid-infrared imaging to access the rest-frame near-infrared emission, where effects from recent star formation and reddening are minimized. *Spitzer* has demonstrated the capability to detect the majority of the host galaxies of high-redshift, far-infrared–selected galaxies (Egami et al. 2004; Ivison et al. 2004; Frayer et al. 2004b; Serjeant et al. 2004; Charmandaris et al. 2004) and promises to be an important tool for further study of this population.

We summarize our main conclusions:

1. We have compiled a large catalog of optical/near-infrared photometry for far-infrared–luminous galaxies selected from deep submm and radio surveys. In total, we have spectroscopic coverage of all 96 galaxies in our sample. Comparing the optical/near-infrared properties of our optically faint radio galaxy

and radio-selected submm subsamples, we find no significant differences between these two populations. This supports the claim that they represent related subsets of the high-redshift far-infrared–luminous galaxy population.

2. We explore the optical–near-infrared and near-infrared colors of these galaxies and show that they span a large range as a function of apparent magnitude or redshift. We attribute this to a wide variation in obscuration and structure within these systems. We demonstrate that signatures of dust are discernible in both the high-resolution imaging from *HST* of these galaxies and their broadband photometry. The complex obscuration suggested by our observations may be a direct result of outflows and winds driving channels surrounding dust, providing a natural explanation for the apparent ease of escape of Lyα photons from these dusty galaxies (Chapman et al. 2004a).

3. We show that typical SMG/OFRGs are physically larger than optically selected galaxies at similar redshifts drawn from magnitude-limited samples. We interpret this as primarily due to the multicomponent nature of the SMG/OFRGs, which in turn reflects the central role of tidal interactions and mergers in triggering the obscured, luminous activity that is used to select the galaxies in our sample. This is confirmed by the clear merger/interacting morphologies shown by a large fraction of galaxies in our sample within the GOODS HDF-N field, which were serendipitously imaged by the *Hubble Space Telescope*.

4. We construct a near-infrared Hubble diagram for our large, homogeneous sample. This shows that the *K*-band luminosities of SMG/OFRGs are typically 1 mag fainter than similarly distant high-redshift, luminous radio galaxies and show a larger scatter than radio galaxy samples (Serjeant et al. 2003). We do not find any statistically compelling evidence that the most bolometrically luminous SMG/OFRGs (those with $>10^{13}\ L_{\odot}$) exhibit a smaller dispersion in their *K*-band magnitudes than the less luminous systems (cf. Serjeant et al. 2003). This is unsurprising given the multicomponent nature of many of these galaxies and the wide range in their rest-frame optical obscuration (Serjeant et al. 2003).

5. The optical–near-infrared colors and near-infrared photometry of SMG/OFRGs show that they are both brighter and redder than UV-selected, star-forming galaxies at either $z \sim 3$ or $\sim$2. We attribute these differences to larger stellar masses and higher obscuration in the SMG/OFRG population, resulting from their more massive progenitors and more active star formation. Simple photometric modeling appears to confirm that the rest-frame SEDs of the SMG/OFRGs indicate continuum reddening at least twice that of the LBG population, and their stellar luminosities may be 5 times larger.

6. We also compare the rest-frame optical properties of these very luminous far-infrared galaxies with similar galaxies in the local universe. We find that these high-redshift galaxies extend the trend for lower optical/far-infrared flux ratios at higher luminosities seen by previous workers, suggesting that an increasing fraction of the activity in these systems is almost completely obscured by dust. The enhancement seen in the far-infrared luminosities of the distant population is also shown by their larger gas masses and higher gas fractions, suggesting a constant star formation efficiency in the most vigorous starbursts out to $z \sim 3$.

7. Finally, we show that if we take the star formation properties of a typical SMG/OFRG from our crude modeling of their rest-frame UV/optical SEDs and let them passively evolve from $z \sim 2.2$, they provide a good fit for the bright end of the luminosity function of morphologically selected spheroidal galaxies in rich clusters at $z \sim 0.5$. This provides additional support for the claims that SMG/OFRGs represent a highly obscured and very active phase in the early evolution of massive elliptical galaxies.

We thank Mark Sullivan for obtaining the *J*/*K*-band imaging of the SA 22 field; Kevin Bundy, Richard Ellis, and Chris Conselice for sharing their HDF-N *K* imaging; and the UKIRT observers who undertook our queue observations. We acknowledge useful conversations or help from Dave Alexander, Omar Almaini, Carlton Baugh, Jon Bird, Colin Borys, Peter Draper, Dave Frayer, Carlos Frenk, Thomas Greve, Bill Keel, Cedric Lacey, Alice Shapley, Jason Stevens, Mark Swinbank, Neil Trentham, and Chris Willott. We thank the referee, Steve Serjeant, for a very constructive report that clarified the discussion and conclusions of this work. I. R. S. acknowledges support from the Royal Society; A. W. B. acknowledges support from NSF grant AST 02-059377, the Research Corporation, and the Alfred P. Sloan Foundation. We acknowledge use of the 2MASS survey data provided through IPAC at Caltech. The Hale 5 m telescope of the Palomar Observatory is owned and operated by the California Institute of Technology. UKIRT is operated by the Joint Astronomy Centre on behalf of the UK Particle Physics and Astronomy Research Council. The AAT is operated by the Anglo-Australian Observatory on behalf of the Australian Research Council and the UK Particle Physics and Astronomy Research Council. This research is based on observations made with the *Hubble Space Telescope* retrieved from the ESO/ST-ECF Science Archive Facility.

REFERENCES

Baugh, C. M., Lacey, C. G., Frenk, C. S., Granato, G. L., Silva, L., Bressan, A., Benson, A. J., & Cole, S. 2004, MNRAS, submitted
Bergstrom, S., & Wiklind, T. 2004, A&A, 414, 95
Bertoldi, F., et al. 2000, A&A, 360, 92
Blain, A. W., Chapman, S. C., Smail, I., & Ivison, R. J. 2004a, ApJ, 611, 52
———. 2004b, ApJ, 611, 725
Bolzonella, M., Miralles, J.-M., & Pello, R. 2000, A&A, 363, 476
Borys, C., et al. 2004, MNRAS, 352, 759
Boyle, B. J., Shanks, T., Croom, S. M., Smith, R. J., Miller, L., Loaring, N., & Heymans, C. 2000, MNRAS, 317, 1014
Capak, P., et al. 2004, AJ, 127, 180
Chapman, S. C., Blain, A. W., Ivison, R. J., & Smail, I. 2003a, Nature, 422, 695
Chapman, S. C., Blain, A. W., Smail, I., & Ivison, R. J. 2004a, ApJ, submitted
Chapman, S. C., Smail, I., Blain, A. W., & Ivison, R. J. 2004b, ApJ, in press
Chapman, S. C., Windhorst, R., Odewahn, S., Yan, H., & Conselice, C. 2003b, ApJ, 599, 92
Chapman, S. C., et al. 2000, MNRAS, 319, 318
Charmandaris, V., et al. 2004, ApJS, 154, 258
Cimatti, A., et al. 2002, A&A, 381, L68
———. 2004, Nature, 430, 184
Clements, D. L., et al. 2004, MNRAS, 351, 447
Cole, S. C., et al. 2001, MNRAS, 326, 255
Croom, S. M., Boyle, B. J., Loaring, N. S., Miller, L., Outram, P. J., Shanks, T., & Smith, R. J. 2002, MNRAS, 335, 459
Daddi, E., et al. 2003, ApJ, 588, 50
———. 2004, ApJ, 600, L127
Dannerbauer, H., Lehnert, M. D., Lutz, D., Tacconi, L., Bertoldi, F., Carilli, C., Genzel, R., & Menten, K. M. 2004, ApJ, 606, 664
de Lucia, G., et al. 2004, ApJ, 610, L77
Dressler, A., et al. 1997, ApJ, 490, 577
Egami, E., et al. 2004, ApJS, 154, 130
Eikenberry, S. S., et al. 2004, WIRC2 Manual (Palomar Mountain: Palomar Obs.)
Ellis, R. S., Smail, I., Dressler, A., Couch, W. J., Oemler, A., Butcher, H., & Sharples, R. M. 1997, ApJ, 483, 582

Erb, D. K., Shapley, A. E., Steidel, C. C., Pettini, M., Adelberger, K. L., Hunt, M. P., Moorwood, A. F. M., & Cuby, J. 2003, ApJ, 591, 101
Ferguson, H. C., et al. 2004, ApJ, 600, L107
Fioc, M., & Rocca-Volmerange, B. 1997, A&A, 326, 950
Franx, M., et al. 2003, ApJ, 587, L79
Frayer, D. T., Ivison, R. J., Scoville, N. Z., Yun, M., Evans, A. S., Smail, I., Blain, A. W., & Kneib, J.-P. 1998, ApJ, 506, L7
Frayer, D. T., Reddy, N. A., Armus, L., Blain, A. W., Scoville, N. Z., & Smail, I. 2004a, AJ, 127, 728
Frayer, D. T., et al. 1999, ApJ, 514, L13
———. 2004b, ApJS, 154, 137
Gear, W. K., Lilly, S. J., Stevens, J. A., Clements, D. L., Webb, T. M. A., Eales, S. A., & Dunne, L. 2000, MNRAS, 316, L51
Genzel, R., Baker, A. J., Tacconi, L. J., Lutz, D., Cox, P., Guilloteau, S., & Omont, A. 2003, ApJ, 584, 633
Giavalisco, M., Ferguson, H. C., Koekemoer, A. M., Dickinson, M., Alexander, D. M., Bauer, F. E., Bergeron, J., & Biagetti, C. 2004, ApJ, 600, L93
Greve, T. R., Ivison, R. J., Bertoldi, F., Stevens, J. A., Dunlop, J. S., Lutz, D., & Carilli, C. L. 2004a, MNRAS, in press
Greve, T., et al. 2004b, MNRAS, submitted
Ivison, R. J., et al. 2002, MNRAS, 337, 1
———. 2004, ApJS, 154, 124
Kim, D.-C., Veilleux, S., & Sanders, D. B. 2002, ApJS, 143, 277
Kochanek, C., et al. 2001, ApJ, 560, 566
Kodama, T., et al. 2004, MNRAS, 350, 1005
Landolt, A. U. 1992, AJ, 104, 340
Leitherer, C., et al. 1999, ApJS, 123, 3
Lilly, S. J., et al. 1999, ApJ, 518, 641
Lutz, D., et al. 2001, A&A, 378, 70
Martini, P., & Weinberg, D. H. 2001, ApJ, 547, 12
Mihos, J. C., & Hernquist, L. 1996, ApJ, 464, 641
Neri, R., et al. 2003, ApJ, 597, L113
Page, M. J., Stevens, J. A., Ivison, R. J., & Carrera, F. J. 2004, ApJ, 611, L85
Pentericci, L., et al. 2001, ApJS, 135, 63
Pozzetti, L., & Mannucci, F. 2000, MNRAS, 317, L17
Sanders, D. B., Soifer, B. T., Elias, J. H., Neugebauer, G., & Matthews, K. 1988, ApJ, 328, L35
Scannapieco, E., & Thacker, R. J. 2003, ApJ, 590, L69
Scoville, N. Z., et al. 2000, AJ, 119, 991
Serjeant, S., Farrah, D., Geach, J., Takagi, T., Verma, A., Kaviani, A., & Fox, M. 2003, MNRAS, 346, L51
Serjeant, S., & Takagi, T. 2004, Nature, submitted
Serjeant, S., et al. 2004, ApJS, 154, 118
Shapley, A. E., Steidel, C. C., Adelberger, K. L., Dickinson, M., Giavalisco, M., & Pettini, M. 2001, ApJ, 562, 95
Smail, I., Chapman, S. C., Ivison, R. J., Blain, A. W., Takata, T., Heckman, T. M., Dunlop, J. S., & Sekiguchi, K. 2003a, MNRAS, 342, 1185
Smail, I., Ivison, R. J., Blain, A. W., & Kneib, J.-P. 1998, ApJ, 507, L21
———. 2002a, MNRAS, 331, 495
Smail, I., Ivison, R. J., Kneib, J.-P., Cowie, L. L., Blain, A. W., Barger, A. J., Owen, F. N., & Morrison, G. E. 1999a, MNRAS, 308, 1061
Smail, I., Morrison, G., Gray, M. E., Owen, F. N., Ivison, R. J., Kneib, J.-P., & Ellis, R. S. 1999b, ApJ, 525, 609
Smail, I., Owen, F. N., Morrison, G. E., Keel, W. C., Ivison, R. J., & Ledlow, M. J. 2002b, ApJ, 581, 844
Smail, I., Scharf, C. A., Ivison, R. J., Stevens, J. A., Bower, R. G., & Dunlop, J. S. 2003b, ApJ, 599, 86
Stanford, S. A., Stern, D., van Breugel, W., & de Breuck, C. 2000, ApJS, 131, 185
Steidel, C. C., Shapley, A. E., Pettini, M., Adelberger, K. L., Erb, D. K., Reddy, N. A., & Hunt, M. P. 2004, ApJ, 604, 534
Stevens, J. A., Page, M. J., Ivison, R. J., Mittaz, J. P. D., Carrera, F. J., Smail, I., & McHardy, I. M. 2004, MNRAS, submitted
Swinbank, A. M., Smail, I., Chapman, S. C., Blain, A. W., Ivison, R. J., & Keel, W. C. 2004, ApJ, in press
Tinney, C., et al. 2004, IRIS2 Manual (Epping: AAO), http://www.aao.gov.au/iris2/iris2.html
Trentham, N., Kormendy, J., & Sanders, D. B. 1999, AJ, 117, 2152
Veilleux, S., Kim, D.-C., Sanders, D. B., Mazzarella, J. M., & Soifer, B. T. 1995, ApJS, 98, 171
Webb, T. M. A., Brodwin, M., Eales, S. A., & Lilly, S. J. 2004, ApJ, 605, 645
Webb, T. M. A., et al. 2003, ApJ, 587, 41
Willott, C., Rawlings, S., Jarvis, M. J., & Blundell, K. M. 2003, MNRAS, 339, 173
Yagi, M. 1998, Ph.D. thesis, Univ. Tokyo